Geosystems and Geoenvironment 2 (2023) 100161

Contents lists available at ScienceDirect

Geosystems and Geoenvironment

journal homepage: www.elsevier.com/locate/geogeo

U–Pb SHRIMP zircon dating and geochemistry of metapelites from the Shillong Meghalaya Gneissic Complex, NE India: Implications for nature of protolith and tectonic setting

Shyam Bihari Dwivedi[a,*], Pratigya Pathak[a], Kevilhoutuo Theunuo[a,b], Ravi Ranjan Kumar[a]

[a] Department of Civil Engineering, Indian Institute of Technology (BHU), Varanasi, India
[b] Geological Survey of India, western region, Jaipur, India

ARTICLE INFO

Article history:
Received 4 June 2022
Revised 11 October 2022
Accepted 6 December 2022

Handling Editor: Vinod Samuel

Keywords:
U-Pb SHRIMP dating
SMGC
Pseudosection
Geochemistry
Metapelites
Columbia assembly

ABSTRACT

The Sonapahar area of Shillong Meghalaya Gneissic Complex (SMGC) is an extension of the Central India Tectonic Zone within the Precambrian Indian shield. The study area mainly consists of metapelites, basic granulites, granitic gneisses and high-grade gneisses as metamorphic imprints. U–Pb SHRIMP zircon dating yields a late Paleoproterozoic age of 1672 ± 6 Ma, which is age of the metapelites protolith. The petrochronology and geochemistry of metapelites and granitic gneiss basement rocks have been studied to learn more about the SMGC's tectonic environment, involvement in the supercontinent cycle, crustal development and geodynamic context. In the NCKFMASHTO system, phase equilibria modelling of metapelites shows peak metamorphic stage at *P-T* conditions of 8.25 kbar/ 820 °C. Cordierite is formed during retrograde metamorphism during the decompression phases. The negative anomalies in Nb, Sr and Ti indicate that crustal sources played a significant role in magmatic emplacement. Geochemical data from metapelites indicate that protoliths were trachy-andesitic in nature, generated during the syn-orogenic environment by subduction tectonism. The SMGC experienced significant tectonic activity throughout the Paleoproterozoic age when the subduction tectonic setting coincided with orogenic activity. The presence of Paleoproterozoic age in the study area, as well as Southwestern Australia and East Antarctica correlates the Sonapahar granulite with the Columbia supercontinent history.

1. Introduction

The Shillong Meghalaya Gneissic Complex (SMGC), a northeastern extension of the Indian peninsular shield which played a significant role in the pioneering discoveries of high pressure (HP) granulite facies metamorphic rocks (Lal et al., 1978; Chatterjee, 2018; Dwivedi et al., 2020). The SMGC is part of the Central Indian Tectonic Zone (CITZ) domain of the Indian peninsula, which was formed during the Satpura orogeny (Desikachar, 1974). These rocks contain evidence of the orogen's geodynamic environment and provide insight into pressures, temperatures and chemical systems. Petrological investigations into various rock types revealed metamorphic conditions ranging from amphibolite to granulite facies (Nandy, 2001; Dwivedi and Theunuo, 2013; Chatterjee, 2018; Dwivedi et al., 2020). Because of their unusual bulk composition, Al-rich metapelites in metamorphic terranes have piqued the interest of geologists. The high-grade metapelites from the SMGC with abundantly developed zircon and monazite have enormous potential for constraining distinct geodynamic evolution. Metapelites with a clockwise *P–T–t* trajectory are an orogenic feature that has been discovered worldwide and is an important component of orogenesis (Harley, 1989). The Shillong Group metasedimentary supracrustal rocks form the NE-SW trending intracratonic Shillong Basin in the Palaeo-Mesoproterozoic age (Mitra, 1998; Bidyananda and Deomurari, 2007). Three distinct age domains (ca. 1571 Ma, ca. 1034 Ma and ca. 478 Ma) are reported within the monazite crystals from the Sonapahar region of the SMGC (Dwivedi et al., 2020). Monazite growth stages are identified when a single grain consists of prominent age domains from the core to the rim portions. The metapelites are affected by three metamorphic stages, which are distinguished by a peak stage followed by two post-peak stages ranging in age from the Mesoproterozoic to the Neoproterozoic. However, there is no evidence for the age of metapelitic protolith has been reported previously, nor has any documentation of the tectonic setting at the

* Corresponding author.
E-mail address: sbd.civ@iitbhu.ac.in (S.B. Dwivedi).

https://doi.org/10.1016/j.geogeo.2022.100161

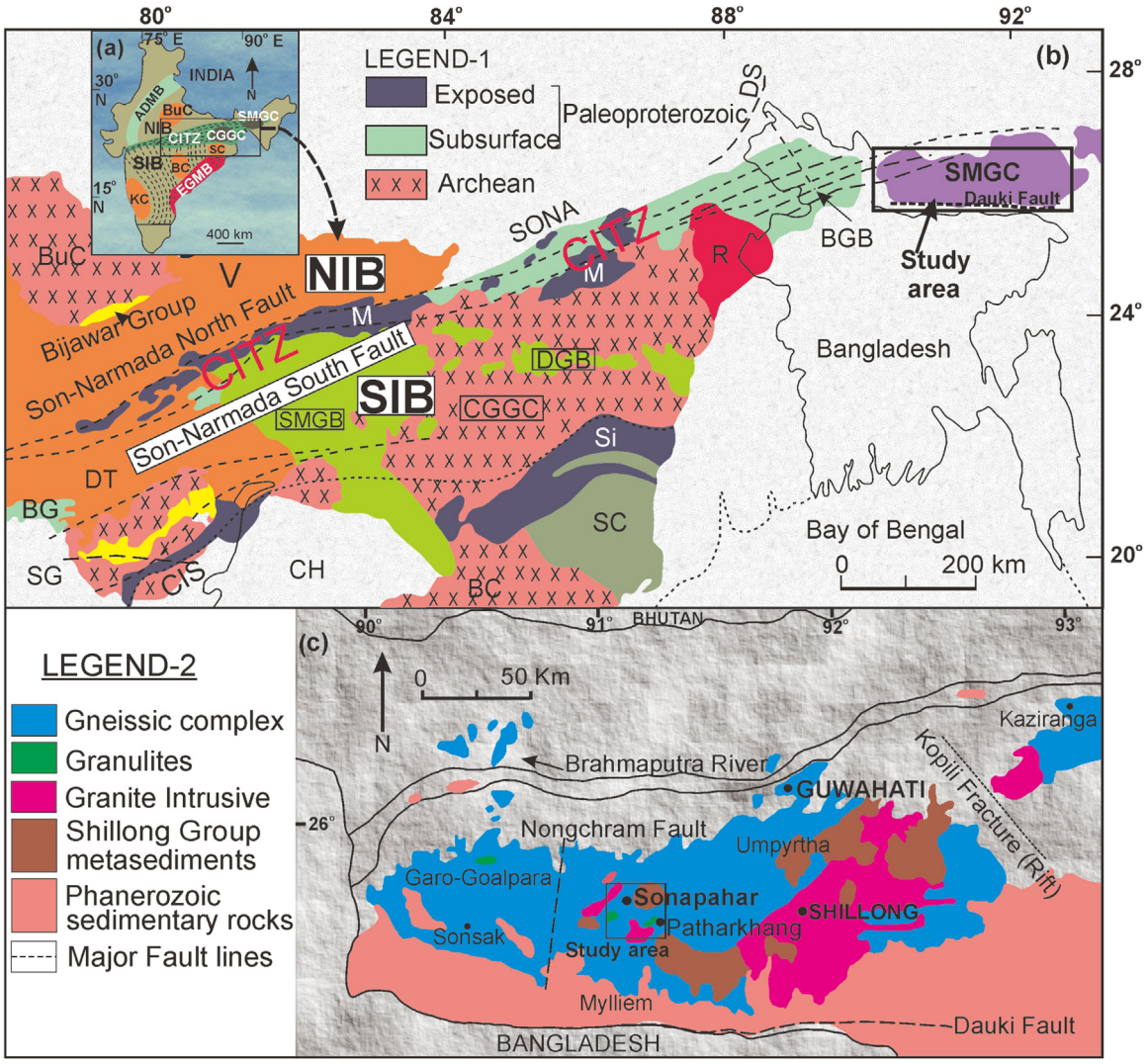

Fig. 1. (a) Inset map showing the location of the Shillong-Meghalaya Gneissic Complex (SMGC) in India. The NIB and SIB contain the archean nuclei of Bundelkhand (BuC) and Singhbhum (SC)-Bastar (BC)-Karnataka (KC), respectively (after Bhowmik et al., 2014). Abbreviations: ADMB, Aravalli-Delhi Mobile Belt; CITZ, Central Indian Tectonic Zone: CGGC, Chhotanagpur Granitic Gneissic Complex; SMGC, Shillong, Meghalaya Gneissic Complex; EGMB, Eastern Ghats Mobile Belt. (b) Geological map shows different lithological units and tectonic elements of the Central Indian Tectonic Zone (CITZ) (after Acharyya, 2003; Hossain et al., 2018). Abbreviations: BC, Bastar Craton; BG, Betul Group; BGB, Barapukuria Gondwana Basin; BuC, Bundelkhand Craton; CGGC, Chotanagpur Granite Gneiss Complex; CH, Chattisgarh; CIS, Central Indian Shear Zone; DGB, Damodar Gondwana basins; DS, Darjeeling-Sikkim Himalaya; DT, Deccan Trap; M, Mohakoshal and equivalents; R, Rajmahal Trap; SG, Sausar Group; SC, Singhbhum Craton; Si, Singhbhum (Paleoproterozoic); SMGB, Son Mahanadi Gondwana basins; SONA, Son Narmada Lineament; V, Vindhyan. The rectangle represents the Shillong-Meghalaya Gneissic Complex located in the western part of NE India. (c) Regional geological map of the Shillong-Meghalaya Gneissic Complex (after Mazumdar, 1976).

time of emplacement. Monazite dating of metapelites yields primarily Palaeo to Mesoproterozoic ages ranging from 1832 to 1596 Ma (Chatterjee et al., 2007, 2011; Chatterjee, 2018). Instead, zircon ages (ca. 2566 Ma and 1758 to 1617 Ma) from older inherited zircon cores of granite gneiss basement rocks suggest reprocessed ancient lithosphere in the formation of proceeding granites (Kumar et al., 2017).

The geochronological tool is used as an accessory mineral zircon, which crystallises from basaltic magma and survives orogenic cycles and other geological processes (Pidgeon and Aftalion, 1978). The geochronological and lithological evidence has resolved several issues, including magmatism timing, craton geodynamic evolution, and transcontinental correlation. Collisional activity assimilated the Columbia supercontinent between ~2000 and ~1800 Ma (Rogers and Santosh, 2002), with peak crustal growth at ca. 1900 Ma (Condie, 2004). Columbia supercontinent had gathered globally where the North China Craton (Tang et al., 2019), the Albany-Fraser Belt of Australia, and the Bunger Hills and the Windmill islands in Antarctica (Harris, 1995) were associated with the Indian peninsular shield, which assembled along the CITZ, formed by a collision of the North and South Indian shields during the Paleoproterozoic age (Yedekar et al., 1990; Bhowmik et al., 2012, 2014). Although, geochronological evidence suggests that CITZ's Paleoproterozoic lithology was reworked in the Mesoproterozoic age, UHT metamorphism was recorded in ca. 2000 Ma (Bhowmik et al., 2005). However, several magmatic episodes occurred in the CITZ between ~2000 and ~1700 Ma (Ray Barman et al., 1990; Acharyya, 2003; Kumar et al., 2021), as well as analogous magmatism in the region of Bangladesh, indicating that Bangladesh's basement is an extended component of the CITZ (Ameen et al., 2007). The CITZ with ENE–WSW trending was formed by a Proterozoic collision (ca. 1600 Ma) between the Southern Indian Block (SIB) and the Northern Indian Block (NIB), with the SIB being subducted beneath the NIB to develop the greater In-

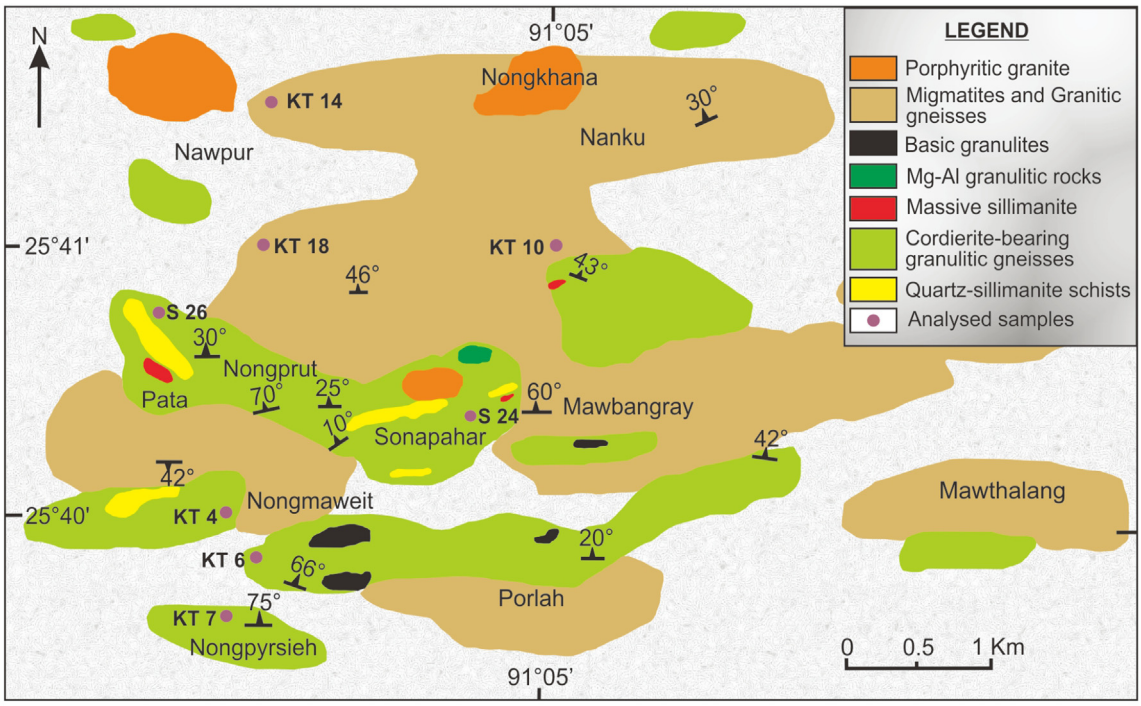

Fig. 2. Geological map of Sonapahar shows different rock types present in the study area (after Dwivedi et al., 2020).

dian landmass (Bhowmik et al., 2012, 2014). Some scholars believe the NIB was dragged southward beneath the SIB (Mishra et al., 2000; Mohanty, 2012; Ozha et al., 2016), while others believe it was double-sided subduction (Naganjaneyulu and Santosh, 2010). The Columbia configuration included the SMGC located between eastern India, southwestern Australia, and east Antarctica.

In this paper, we use a combination of U–Pb SHRIMP geochronology, bulk-rock geochemical analysis and phase equilibria modelling to suggest age and nature of the protolith as well as the tectonic setting for metapelites and granite gneiss basement rocks. The petrographic analysis reveals that the metapelites' mineralogical developments are linked to various metamorphic events. However, the geochemical affinity of these rocks in terms of their tectonic environment is completely unknown to date, and this research suggests the results of the geochemical investigation of the rocks. The isothermal decompression is predicted by the evolutionary tendency of metapelites. Furthermore, all interpretations have been utilised to connect these data to infer that this region was part of an active continental margin connected with the Columbian supercontinent.

2. Geological setting and previous geochronological studies

The Shillong-Meghalaya-Gneissic Complex (SMGC) is 47,000 km^2 in size and is bordered in the north by the Brahmaputra River and the Main Boundary thrust, while the Dauki Fault separates it in the south (Fig. 1). The Jamuna fault is situated in the western part, and the Indo–Myanmar Mobile Belt is located in the eastern part (Acharyya et al., 1986). The Shillong Plateau in Meghalaya and the Mikir Hills Plateau in Assam, represent Precambrian rocks in northeastern India. The archean basement gneissic complex and migmatitic granitoids build up the SMGC. The SMGC has metamorphic rocks that lie unconformably above the basement gneissic complex, ranging from greenschist to granulite facies (Nandy, 2001). Low-grade metasediments from the greenschist facies and a simple metamorphic history characterise the Shillong Group. Within the Shillong Group of metasediments, basic volcanics known as Khasi green stones, appear as concordant and discordant bodies (Mazumder, 1986). Epidiorite and hornblende schist are small intrusive metamorphosed entities found in Khasi greenstone that often have relict minerals or textures indicating volcanic origin (Srivastava et al., 2019).

Proterozoic granite gneisses, granitoids and migmatites dominate the Meghalaya plateau, which is overlain by Shillong Group metasedimentary rocks (Mazumdar, 1976). The Sonapahar region consists of different types of metamorphic assemblages, including garnet-bearing and garnet-absent metapelites, non-garnetiferous basic granulites, quartz-sillimanite gneisses, and calc-silicate gneisses (Fig. 2; Lal et al., 1978; Dwivedi and Theunuo, 2013; Chatterjee, 2018; Dwivedi et al., 2020). Metapelites coexist with granitic gneisses and have grading contact with one another. The leucosome layers are frequently observed along the contact of the metapelites and granitic gneisses. In contrast, the SMGC reported silica-deficient sapphirine–bearing granulites and calc-silicate gneisses occur as enclaves within granite basements and have banding features (Lal et al., 1978). Instead of these rocks, migmatites, cordierite-sillimanite gneisses, massive sillimanite rocks, Wagnerite-bearing Mg-Al granulites and two-pyroxene bearing mafic granulites occur as small irregular pockets in granite gneisses (Dwivedi and Theunuo, 2011, 2017).

The SMGC has few petrochronological evidence and the data from basement rock is largely Mesoproterozoic in age. The SMGC basement gneisses were dated between ~1714 and ~1150 Ma, implying that they were involved in the accretion and fragmentation of the Columbia and Rodinia (Ghosh et al., 2005). Chatterjee et al. (2007) discovered a monazite age of ca. 1596 Ma in the Goalpara region, as well as three significant age domains of ca. 1472 Ma, ca. 1078 Ma and ca. 500 Ma in the Sonapahar, with the younger age of ca. 500 Ma correlating to the granitoid that intruded the SMGC's east-central section. Dwivedi et al. (2020) also identified three domains from the same study area, including ca. 1571 Ma, ca. 1034 Ma and ca. 478 Ma, however, the protolith's age was not revealed. The SMGC was part of the eastern extension of the CITZ during the Paleoproterozoic (ca. 1700 Ma), and

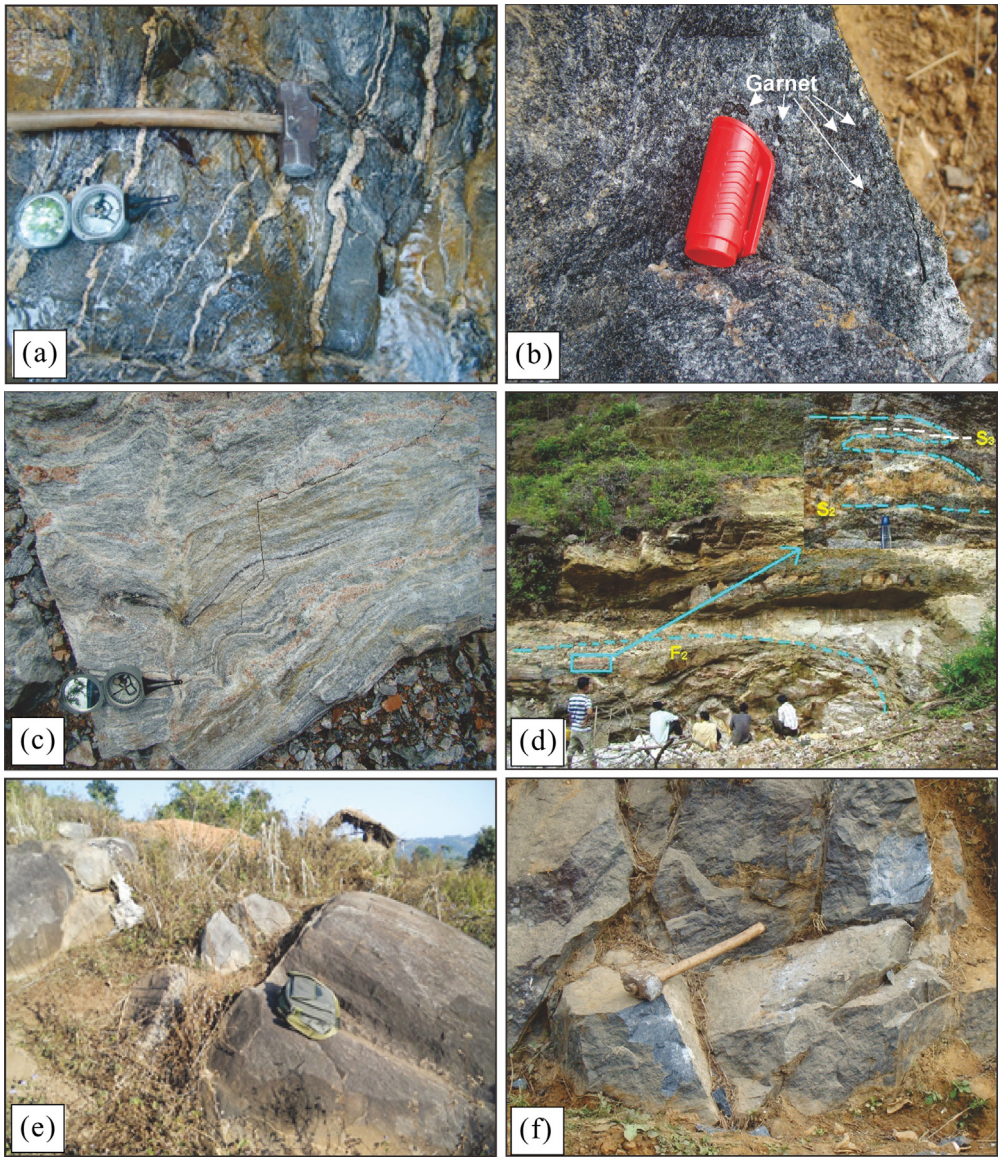

Fig. 3. Field photographs from the Sonapahar region shows: (a) distinct quartzo-feldspathic leucosomes cutting across the metapelites; (b) pink garnets appeared on the surface of metapellites, and cordierite found in the form of blue-purple grain; (c) thin lamillea of leuco-melanosomes present and frequently accompanied by coarse biotite flakes in parallel orientation; (d) deformation with the development of schistosity and crenulation cleavage; (e) outcrop and (f) close view of granitic gneiss basement rocks.

it was attached to the Columbia supercontinent (Hossain et al., 2007). Despite the fact that geochronological evidence suggests that the CITZ's Paleoproterozoic lithology was reworked in the Mesoproterozoic, UHT metamorphism was reported in ~2000 Ma (Bhowmik et al., 2005). Furthermore, various magmatic events occurred in the CITZ between 2000 and 1700 Ma (Acharyya, 2003). The Pb-Pb zircon ages of basement gneisses from Umling (ca. 1580 Ma), Riangdo gneisses (ca. 1451 Ma), charnockite (ca. 1284 Ma and ca. 1077 Ma) and quartzite (ca. 1979 Ma and ca. 1617 Ma) were reported by Bidyananda and Deomurari (2007). These data correspond to the Eastern Ghat Belt, which is affected by various thermal activities. The zircon dating recognized three events of magmatism (~1500, ~1000 and ~500 Ma) in the SMGC (Yin et al., 2010), which are congruent with metamorphism (Dwivedi et al., 2020).

2.1. Local geology

The area of investigation around the Sonapahar (Latitude 25º39' to 25º42' N and Longitude 91º01' to 91º07' E) has been covered under the Geological Survey of India Toposheet No. 78 O/2 on a 1:50,000 scale (Fig. 2). It is located in the SMGC's central region, some 40 km northwest of Nongstoin City. The Sonapahar (new name Riangdo) region comprises upper amphibolite to granulite facies rocks and is located in Meghalaya's West Khasi Hills. Although, the Sonapahar region is part of the Shillong plateau and an extended stretch of the Indian peninsula in the northeast; nonetheless, the Garo–Rajmahal depression separates the Sonapahar from the Indian peninsular shield (Evans, 1964). Dunn (1929) was the first to create a detailed map of the area surrounding Sonapahar, and many others followed suit. As a result, the Sonaphar has identified a number of economically significant sites. These metapelites are typical of granulite-facies rocks that have been studied in depth by petrolography. Therefore, petrological and geochemical criteria are used to infer the geodynamic development of the lithosphere, which is valid for all rock entities present within the terrane at the time. The Sonapahar region is noted for its less number of granulite-facies rocks since the basement rocks have only been exposed in a small part of the Shillong plateau (Lal et al., 1978; Dwivedi and Theunuo, 2017).

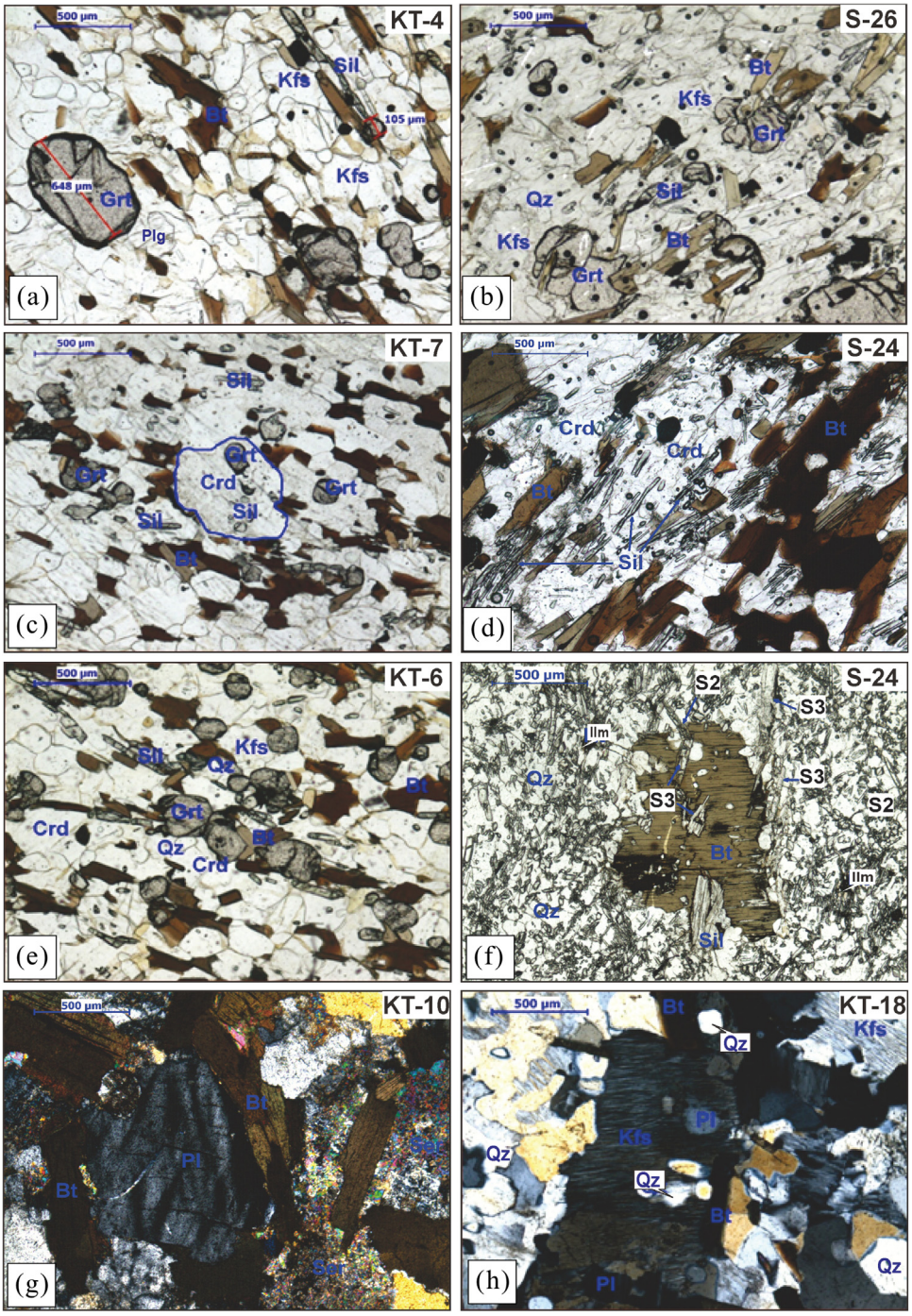

Fig. 4. (a) Xenoblastic grains of garnet (0.1 to 0.6 mm) in diameter of metapelite (In plane polarized light). (b) Small grains of garnet associated with cordierite, sillimanite and biotite in metapelite (In ppl). (c) Photomicrograph of cordierite grain with sillimanite and garnet as inclusion (in ppl). (d) Trails of sillimanite needles defining S_i within cordierite porphyroblasts and merging into S_e (=S_2), suggesting post tectonic crystallization of cordierite in metapelite (in ppl). (e) Photomicrograph of metapelite showing essentially granoblastic mosaic texture (in ppl). (f) Coarse porphyroblast of biotite containing two sets of trails of sillimanite needles: (i) parallel to the S_3 foliation at the core and along the rim and (ii) parallel to relic S_2 foliation discordant with S_3 (in ppl). (g) Biotite flakes wrap around the plagioclase grain in granitic gneisses (in ppl). (h) Perthitic k-feldspar with plagioclase and biotite exhibiting quadrille structure in granitic gneisses (in ppl).

2.2. Field relationships

Granitic gneiss is found as basement rock at the outcrop scale. Metapelites and granitic gneisses form a cross-cutting interaction in some areas, with several thin distinct leucosomes intruding into the Metapelites. The researched area's extensive petrographic analysis reveals several rock types and their mineral correlations (Dwivedi et al., 2020). The textural properties and reaction relationships of the minerals have been investigated, and an attempt has been made to deduce the various stages of deformation and metamorphic crystallisation of these rocks. Massive and dark grey metapelites with predominantly medium-grained quartzo-feldspathic leucosomes cut through the metapelites in varying quantities; the presence of leucosomes in the metapelites is indicative of the presence of liquid or melts (Fig. 3a). Pink garnets of medium size are found on the surface of metapelites, where

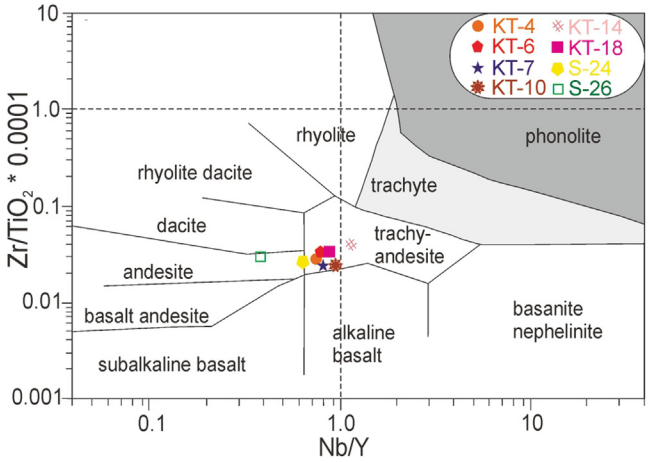

Fig. 5. The chemical classification and nomenclature of metapelites and granitic gneisses based on the immobile trace elements: Nb/Y vs. Zr/TiO_2 (Winchester and Floyd, 1977).

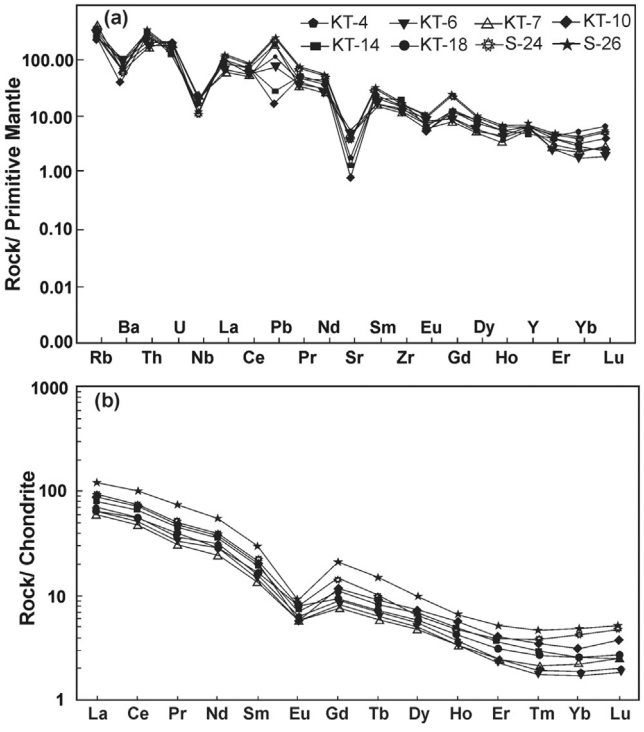

Fig. 6. (a) Primitive mantle normalized multi-elements spider diagram of metapelites and granitic gneisses (Sun and McDonough, 1989). (b) Chondrite normalized REE plot (Sun and McDonough, 1989) showing uniform and nearly horizontal REE pattern.

cordierite is found as blue-purple grain that passes across the rocks (Fig. 3b). Laminar structures appear in some sections, with thin lamillea of leuco-melanosomes present and frequently accompanied by coarse biotite flakes in parallel orientation (Fig. 3c). Structural events developed during metamorphic episodes are used as a time indicator for metamorphic crystallization. These events are categorized as first-generation fold (F_1). During the first phase of deformation D_1 related to S_1 schistosity, giving rise to axial-plain foliation S_2 and the second generation micro-fold F_2 during deformation D_2 with the development of crenulation cleavage S_3 (Fig. 3d). The relationship between the fabric of the rock or external schistosity (S_e) and the internal trails or internal schistosity (S_i) of the porphyroblast is also considered for the chronological study of crystallization and deformation. Granitic gneisses are intermediate to coarse-grained, light grey to white in colour, and their texture shows that crystallisation occurred during deformation after annealing outlasted the deformation (Fig. 3e and f).

3. Analytical techniques

3.1. Petrography

We collected over twenty seven representative samples of metapelites and granitic gneisses from the Sonapahar area during different field work sessions. At IIT (BHU)'s Engineering Geosciences lab, we prepared thin sections of collected samples and examined them with an LEICA DM 2500 polarising microscope. A thorough petrographic analysis and textural association revealed a diverse range of mineral assemblages. Simultaneously, we chose some representative samples for further examination.

3.1.1. Metapelites

The Sonapahar region consists of a variety of metapelite samples (KT–4, KT–6, KT–7, S–24 and S–26), the modal percentages of which are shown in Table 1. The petrography and mineral chemistry of several types of metapelites have been thoroughly examined (Dwivedi et al., 2020). Metapelites are mostly composed of garnet, biotite, cordierite, sillimanite, plagioclase, K-feldspar and quartz, with accessory minerals of magnetite, ilmenite, zircon and monazite. In metapelite KT-4, garnet grains varies in size from 0.2 to 0.8 mm in diameter and have a unique isotropic optical characteristic in polarised light (Fig. 4a). They are always present in small to medium xenoblasts and are usually present in intermittent amounts. In metapelite S-26, garnet has quartz and biotite inclusions, as well as some sillimanite needle trails, and the S_i of

Table 1
Summary of approximate modal composition (in percentage) of the metapelites (KT-4, KT-6, KT-7, S-24 and S-26) observed under a petrological microscope through Lieca-Qwin software.

Sample	Modal%							
	Grt	Crd	Sil	Bt	Pl	Kfs	Qz	Opq
KT-4	18	29	4	9	18	9	10	4
KT-6	22	20	7	11	12	10	13	5
KT-7	11	32	5	10	8	12	19	3
S-24	–	24	14	27	12	11	7	5
S-26	37	–	7	18	14	9	10	5

garnet merges into S_e, or the exterior schistosity S_2 (Fig. 4b). The textural relationship indicates that prograde garnet formed by following metamorphic reaction:

$$\text{Biotite} + \text{quartz} \rightarrow \text{garnet} + \text{K} - \text{feldspar} + \text{melt} \quad (1)$$

$$\text{Biotite} + \text{sillimanite} + \text{quartz} \rightarrow \text{garnet} + \text{K} - \text{feldspar} + \text{melt} \quad (2)$$

In metapelite KT-7, cordierite includes xenoblastic to subidioblastic garnet, elongated crystals of sillimanite and quartz as inclusion (Fig. 4c), this textural relationships point to a metamorphic process:

$$\text{Garnet} + \text{sillimanite} + \text{quartz} \rightarrow \text{cordierite} \quad (3)$$

Metapelite (S-24) can be defined as a medium-grained mosaic of garnet porphyroblasts, K-feldspar and plagioclase, while well-orientated biotite flakes develop with needles of sillimanite. Cordierites are poikiloblastic and contain inclusions of biotite and sillimanite merging into the external foliation (S_e), such as S_2 and S_3 foliation (Fig. 4d). In metapelite KT-6, garnet, biotite and sillimanite are merged within the cloud of cordierite that demarcates

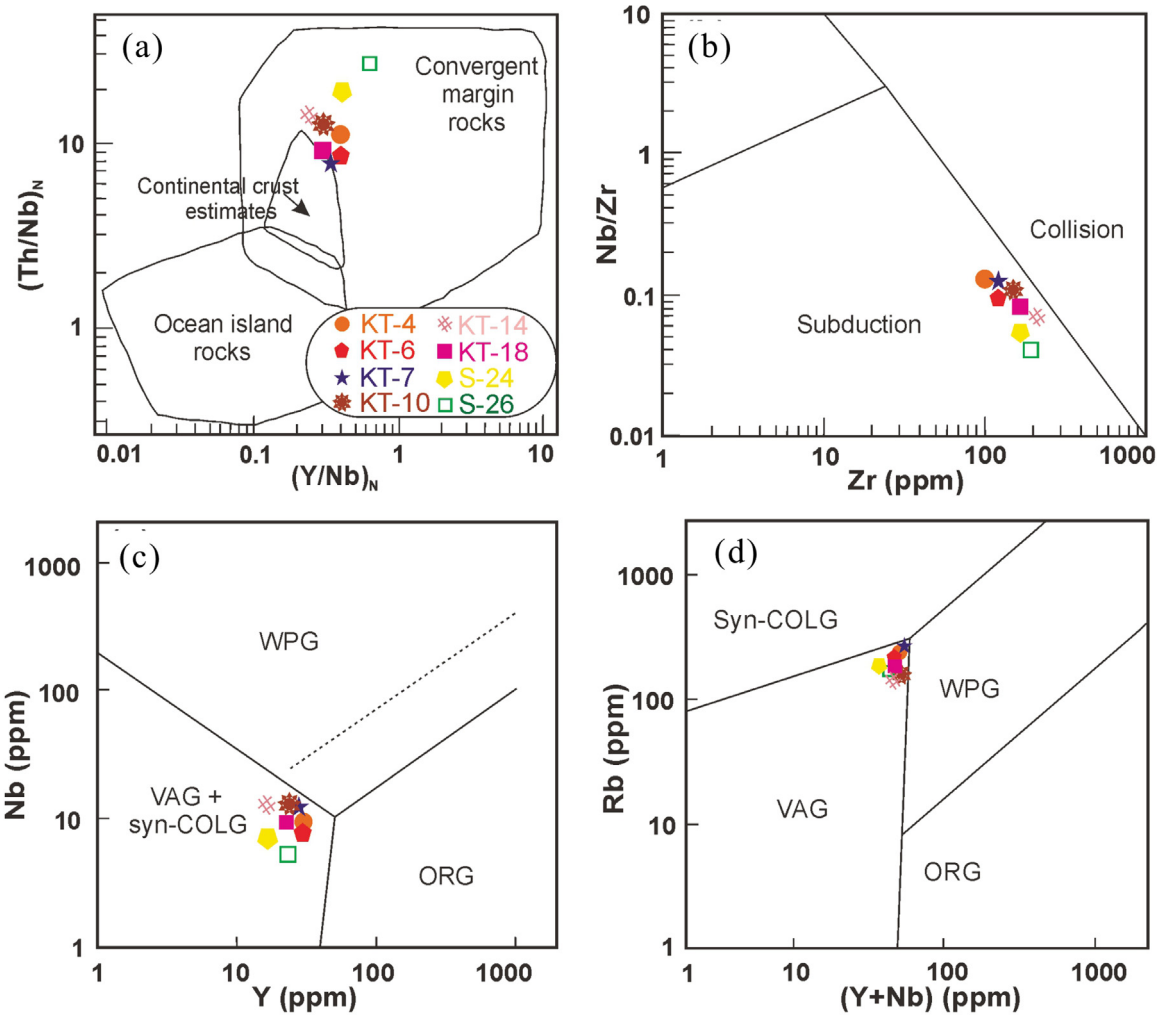

Fig. 7. (a) $(Y/Nb)_N$ vs. $(Th/Nb)_N$ diagram used to discriminate tectonic regimes of metapelites and granitic gneisses from the Sonapahar of the SMGC (Moreno et al., 2014). (b) Zr vs. Nb/Zr discriminate diagram used to discriminate tectonic regimes (Thieblemont and Tegyey, 1994). (c) Y vs. Nb tectonic discrimination diagram (Pearce et al., 1984) plotted with metapelites and granitic gneisses, mostly showing an affinity towards the volcanic arc granite and syn-collisional granite (VAG + syn-COLG). (d) (Y + Nb) vs. Rb tectonic discrimination diagram (Pearce et al., 1984) plotted for metapelites and granitic gneisses. Syn-COLG: syn-collisional granite; WPG: within plate granite; VAG: volcanic arc granite; ORG: ocean ridge granite.

the external foliation (S_e) such as S_2 foliation (Fig. 4e) suggesting the reaction:

$$\text{Biotite} + \text{sillimanite} + \text{quartz} \rightarrow \text{cordierite} + \text{K} - \text{feldspar} + \text{melt} \quad (4)$$

Coarse porphyroblasts of biotite with trails of sillimanite define the internal schistosity (S_i), which merges with the external schistosity S_e equivalent to S_2 foliation. The sillimanite inclusions at the core of some coarse biotite flakes lie at an oblique angle and are concordant with the S_3 foliation trend of the matrix at the rim of the biotite grain (Fig. 4f). The feature suggests post-tectonic crystallization of biotite with respect to S_2 and slight rotation during D_2 deformation which is followed by post-tectonic recrystallization.

3.1.2. Granitic gneisses

The porphyritic granitic gneissic rocks have been widely exposed in and around the Sonapahar region. The rocks with a higher feldspar and quartz mineral content are lighter in colour. However, when the proportion of biotite increases, the colour darkens, and little plagioclase crystallises in small melt pockets inside porphyroblast feldspar. They normally have a gneissose structure, but they can also have vast dense foliated fabrics. The fabric is primarily gneissose with different foliations, with parallel and laminar alignment of biotite flakes (Fig. 4 g). K-feldspar is primarily hair perthite, with plagioclase blebs forming quadrille structures inside the mineral (Fig. 4h). Inclusions of rounded quartz and plagioclase can be seen in coarse K-feldspar porphyroblasts.

3.2. Whole-rock analytical technique

Five metapelite samples (KT–4, KT–6, KT–7, S–24 and S–26) and three granitic gneissic samples (KT–10, KT–14 and KT–18) were analysed for major, trace, and REE at the Wadia Institute of Himalayan Geology (Dehradun), India. To prevent contamination, fresh sample chips were manually powdered with an agate mortar. The X-ray fluorescence (XRF) method was used on sample pellets to determine major and trace elements using the Siemens SRS 3000/S-8 tiger sequential X-ray spectrometer with a window Rh X-ray tube. The analytical accuracy is better than 12% for trace elements and 5% for major oxides. On repeated measurements, accuracy is better than 2% of the maximum observed standard deviation (Saini et al., 1998). ICP-MS (Perkin-Elmer SCIEX) was used to analyse rare earth elements (REE); the sample was dissolved in Teflon beakers using the open digestion method with HF-HNO_3-

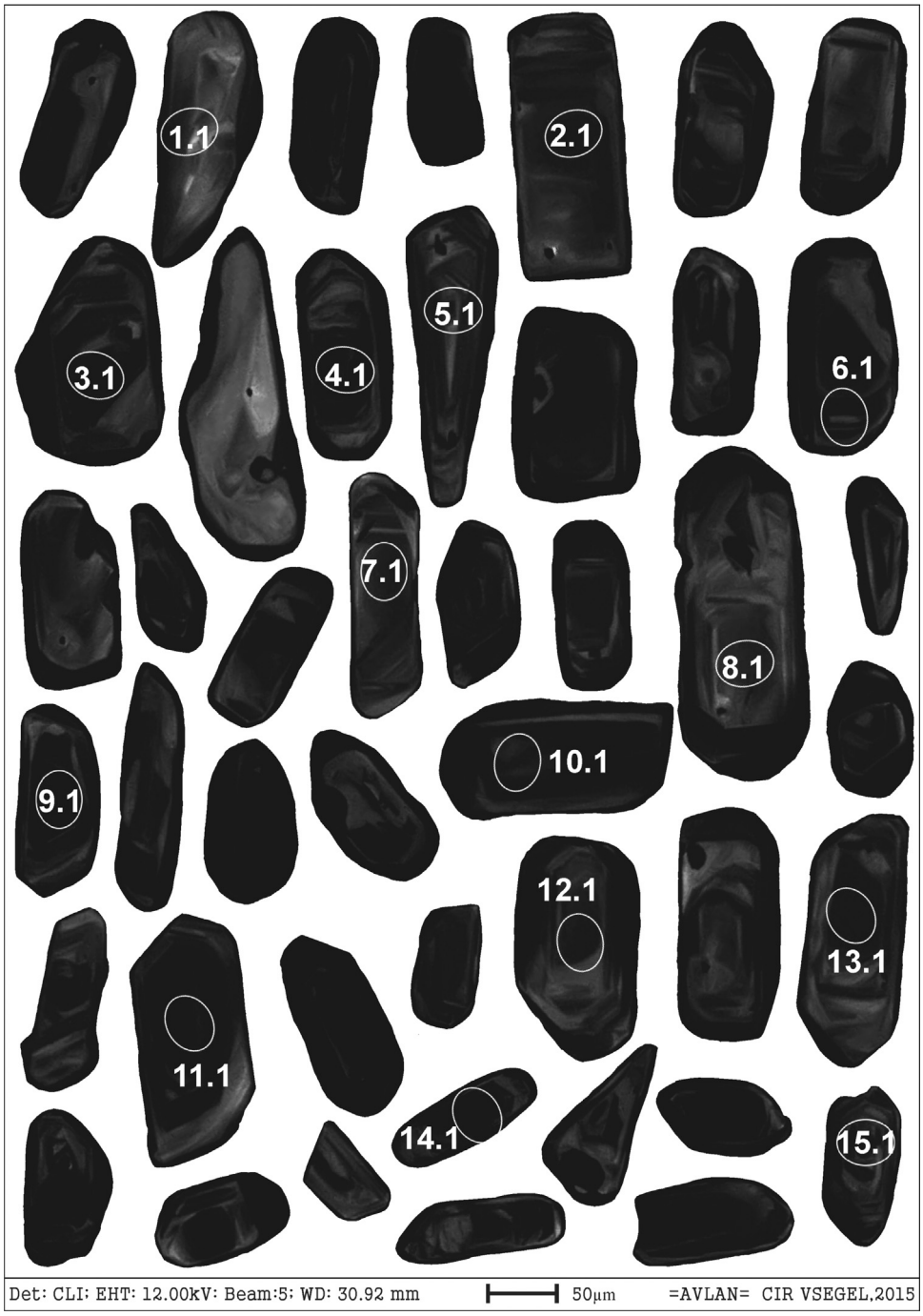

Fig. 8. (a) Representative cathode-luminescence (CL) images of zircons and $^{206}Pb/^{238}U$ ages of analysed spots (circles) of zircons with different zoning patterns from metapelites of the Sonapahar region.

$HClO_4$; after boiling, it was allowed to oxidise and dry; the residue was then dissolved in 10% nitric acid. For most REE elements, the relative standard deviation (RSD) is less than 10% (Khanna et al., 2009).

3.3. U-Pb Shrimp zircon analytical technique

The zircon SHRIMP dating was carried out at Isotopic Geochemistry Laboratory in Canada, where zircons were separated from metapelite rock sample (KT-4). The zircon crystals were mounted in epoxy together with TEMORA (Middledale Gabbroic Diorite, New South Wales, Australia) and 91,500 (Geostandard zircon, Wiedenbeck et al., 1995) reference zircons. The grains were polished until they were halved. Cathodoluminescence (CL) images were taken for all analytical spots from zircon crystals, which were carefully selected based on fracture distribution and zoning patterns. The U-Pb content of zircons was determined using SHRIMP-II. The analytical spot was 10–20 μm in size, similar to the primary ion beam. SQUID 2.50 and Isoplot 3.70 version 4.0 were used to plot the ages in Concordia-Discordia and probability density diagrams (Ludwig, 2011).

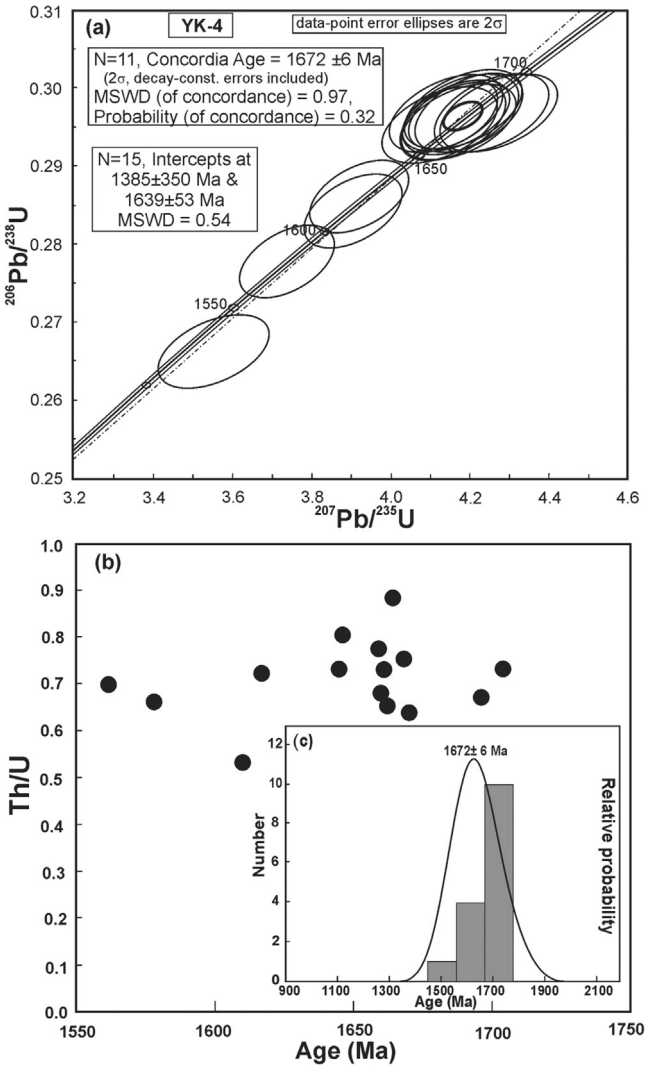

Fig. 9. (a) U-Pb Concordia diagram shows a mean crystallization age (1672 ± 6 Ma) of zircons (intercepts at 1385 ± 350 Ma and 1639 ± 53 Ma). (b) Th/U vs age plot ($^{207}Pb/^{206}Pb$ near-concordant dates). (c) The age spectrum has shown by the probability density plot with a prominent peak at 1672 ± 6 Ma.

3.4. Phase equilibria modelling

Based on mineral assemblages, *P-T* pseudosection has been calculated for metapelite (KT-4) in the NCKFMASHTO system with the help of Perple_X v.6.7.1 (Connolly, 2005, 2009). According to petrographic studies, the metapalitic sample (KT-4) contains the most mineral phases including garnet, biotite, sillimanite, cordierite, plagioclase, quartz, K-feldspar, ilmenite and magnetite, and was thus chosen for pseudosection study. We employed various solid solution models in the phase diagram: garnet, melt and biotite (HP: Powell and Holland, 1999); cordierite (W: White et al., 2007); ilmenite (WPH: White et al., 2000); plagioclase (JH: Holland and Powell, 2003). The mineral abbreviations have been taken from Whitney and Evans (2010). The calculations for P-T-X pseudosection modelling using all input bulk compositions, solution models, and assumptions are provided in the Supplementary Data, Appendix A.

4. Geochemistry

The whole-rock geochemical analysis of the metapelites and granitic gneisses are represented in Table 2. Because the alkalies tend to be mobilised during weathering and metamorphism, metapelites and granitic gneisses are classified using the immobile trace element Zr/Ti vs. Nb/Y classification diagram (Winchester and Floyd, 1977; Fig. 5). This plot reveals metapelites and granitic gneisses lie in the trachy-andesite to andesite field. The incompatible trace elements (Rb, Ba, Sr, Zr, Y, Th and U) are predominate, with a lower content of compatible elements (Cr, Ni, *Sc* and Co). The vast range of LFSE elements could be attributable to different degrees of motion of the elements during protolith transformation and metasomatism. The high Ba concentration indicates that the source was abundant in K-feldspar.

The relative abundances of Rb, Th and Pb, as well as depletion in Ba, Sr, Nb and Ti, were shown in the spider diagram (Sun and McDonough, 1989; Fig. 6a). The ilmenite mineral phases in the rock samples are responsible for the Ti and Nb depletion. The Zr concentration varies from 125 to 198 parts per million (ppm), which can be explained by the modal percentage of zircon in different samples. The Th/U ratio ranges from 3.26 to 9.96, reflecting oxidation conditions during the depositions of pelitic rocks (McLennan and Taylor, 1980). Each element is organised in a uniform, and nearly horizontal REE pattern in the Chondrite normalised REE plot. With the exception of La, Ce and Nd, which have larger ranges of 41.3–83, 84.7–173 and 33.8–74 ppm, respectively, the variance in abundances of these elements is relatively small. Although the REE pattern in metapelites and granitic gneisses is fractionated, light rare earth elements (LREE) have natural abundances, and Eu ($Eu_N/Eu^* = 0.37–0.62$) has negative anomalies for both metapelites and granitic gneisses. The La_N/Lu_N ratio of LREE to HREE ranged from 10.57 to 34.16, indicating depletion in the HREE pattern (Fig. 6b).

The trace-element data are used to create various tectonic discrimination diagrams that highlight the type of tectonism and the nature of the magmatic source. The metapelites and granitic gneisses show convergent margin setting on the $(Y/Nb)_N$ vs. $(Th/Nb)_N$ plot (Fig. 7a: Moreno et al., 2014), while the Zr vs. (Nb/Zr) plot shows subduction setting (Fig. 7b; Thieblemont and Tegyey, 1994). The Y vs. Nb diagram (Pearce et al., 1984) reveals that the syn-orogenic environment and source characters are volcanic arc granite and syn-collisional granite setting (VAG + Syn-COLG) (Fig. 7c). In contrast, the Rb vs. (*Y* + Nb) diagram (Fig. 7d) demarcates affinity for the volcanic arc granite (VAG) of metapelites and granitic gneiss basement rocks.

5. U–Pb Shrimp zircon geochronology

The analytical results of U–Pb SHRIMP zircons dating of metapelites (KT–4) are listed in Table 3, and all zircon grains are shown in Fig. 8. Most crystals are euhedral to subhedral, with length and breadth ranging from 70 to 100 μm and 20 to 30 μm, respectively. The CL images are used to assess the shape, size and zoning pattern along with the structure of zircon crystals. The measurements were taken on large core or mantle sections. The dark CL core with oscillatory zoning is surrounded by a brighter CL rim with homogeneous overgrowth in most of these zircon crystals. Out of the fifteen analytical spots of zircons, thirteen spots range from 1667 ± 10 Ma to 1678.1 ± 10 Ma of $^{207}Pb/^{206}Pb$ age, whereas the two zircon spots on YK–4.8.1 and YK–4.9.1 are comparatively of a younger age 1562 ± 27 and 1578 ± 21, respectively. The Th/U ratio ranges from 0.47 to 0.88. The Concordia age is 1672±6 Ma at 2σ decay–constant errors with MSWD (of concordance) = 0.97 and Probability (of concordance) = 0.32, according to the Tera-Wasserburg Concordia diagram (Fig. 9a), which is based on fifteen studied zircons and shows all data near the Concordia line. The zircon crystals show a low degree of discordance (–1 to 3%), with a lower intercept age of 1385 ± 350 Ma and upper intercept age of 1639 ± 53 Ma, with MSWD = 0.54. A younger age clus-

Table 2
Major oxides, trace elements and REEs data of the metapelites from Sonapahar.

Oxides	KT-4	KT-6	KT-7	KT-10	KT-14	KT-18	S-24	S-26
Location	N25º40'02" E91º05'36"	N25º39'52" E91º05'31"	N25º39'42" E91º05'37"	N25º40'51" E91º05'01"	N25º41'45" E91º05'48"	N25º41'16" E91º05'44"	N25º40'32" E91º05'13"	N25º40'46" E91º05'42"
SiO_2	63.49	66.96	64.34	63.63	65.72	63.81	62.83	62.33
Al_2O_3	17.58	15.85	16.91	18.81	18.49	17.16	16.39	15.96
Fe_2O_3	5.99	5.56	6.12	6.69	6.50	5.76	7.66	7.81
TiO_2	0.47	0.53	0.51	0.60	0.54	0.51	0.69	0.67
MnO	0.10	0.04	0.09	0.05	0.06	0.10	0.09	0.09
MgO	2.95	2.46	3.15	5.47	3.77	3.85	4.39	4.91
CaO	0.90	0.93	0.65	0.11	0.16	0.97	1.04	1.34
Na_2O	2.26	2.19	1.63	0.14	0.61	2.45	1.64	1.91
K_2O	3.65	3.52	4.07	1.94	2.49	3.44	3.87	3.26
P_2O_5	0.04	0.04	0.05	0.05	0.02	0.04	0.09	0.07
LOI	0.73	0.70	0.90	0.96	0.74	0.77	0.66	0.86
Total	98.16	98.78	98.42	98.45	99.10	98.86	99.75	99.21
Mg#	0.49	0.47	0.50	0.62	0.53	0.57	0.56	0.59
Trace Elements (ppm)								
LFSE-LILE								
Ba	418.0	432.0	406.0	262.0	682.0	574.0	487.0	461.0
Rb	232.0	227.0	253.0	162.0	159.0	192.0	197.8	171.7
Sr	101.0	122.0	103.0	17.0	28.0	122.0	92.0	99.0
Transitional Elements								
Cr	58.0	52.0	60.0	97.0	57.0	50.0	87.0	97.0
Ni	27.0	30.0	34.0	39.0	49.0	34.0	35.7	29.4
V	69.0	66.0	74.0	113.0	82.0	63.0	60.0	62.0
Zn	136.0	28.0	129.0	72.0	62.0	176.0	114.4	119.7
Co	6.2	24.4	7.8	30.8	23.0	4.0	14.0	17.0
HFSE								
Y	29.0	28.0	29.0	28.0	23.0	27.0	21.0	29.9
Nb	14.0	14.0	15.0	15.0	15.0	14.0	9.4	8.4
Zr	118.0	144.0	125.0	142.0	213.0	153.0	175.0	198.0
Sc	13.0	14.4	12.1	17.2	15.1	11.5	15.0	15.1
Cu	55.0	4.0	39.0	21.0	8.0	47.0	47.8	83.6
Pb	34.0	13.0	34.0	3.0	5.0	21.0	39.5	35.4
Th	17.0	14.0	14.0	21.0	24.0	15.0	21.2	27.9
U	4.3	4.0	4.3	3.7	2.4	3.6	3.6	2.8
Ga	22	15	21	20	20	24	19.2	18.2
REE								
La	46.10	44.40	41.30	59.20	53.80	46.90	56.00	83.00
Ce	95.60	93.30	84.70	125.30	115.50	98.90	116.00	173.00
Pr	10.40	9.50	8.60	12.80	12.50	11.00	14.00	20.00
Nd	39.60	38.40	33.80	51.90	48.20	40.30	52.00	74.00
Sm	7.16	6.45	5.90	9.03	8.38	7.57	9.34	13.20
Eu	1.22	0.99	1.03	0.97	1.20	1.34	1.57	1.61
Gd	5.73	4.99	4.53	6.96	6.46	5.77	8.94	12.61
Tb	0.87	0.68	0.64	0.99	0.89	0.80	1.11	1.63
Dy	5.05	3.60	3.50	5.54	4.95	4.33	4.85	7.09
Ho	0.91	0.55	0.56	0.92	0.81	0.70	0.76	1.06
Er	2.26	1.10	1.19	1.97	1.74	1.50	1.90	2.48
Tm	0.38	0.13	0.16	0.26	0.22	0.20	0.29	0.35
Yb	2.69	0.86	1.10	1.55	1.26	1.27	2.10	2.40
Lu	0.47	0.14	0.19	0.28	0.19	0.21	0.35	0.38
ΣREE	218.44	205.09	187.20	277.67	256.10	220.79	271.14	398.16
Eu_N/Eu^*	0.58	0.53	0.61	0.37	0.50	0.62	0.53	0.38
La_N/Lu_N	10.57	34.16	23.41	22.77	30.50	24.06	17.23	23.53

CIA = $[Al_2O_3/ (Al_2O_3 + CaO + Na_2O + K_2O)]*100$
ICV = $(Fe_2O_3 + K_2O + Na_2O + CaO + MgO + TiO_2)/ Al_2O_3$.

ter contains fewer data points, yet we have a large amount of computed error. The upper intercept age reflects the protolith age, and a subsequent thermal metamorphic event happened at a younger age, which might or could not have occurred at ca. 1385 Ma. The U and Th values range from 201 to 448 and 130 to 335 ppm, respectively, implying numerous generating sources (Fig. 9b). The Isoplot (Ludwig, 2011) of this rock has plotted the age distribution of the probability density diagram (Fig. 9c).

6. *P-T* conditions

6.1. Geothermobarometry

The *P-T* conditions of metapelites were calculated by several software tools, including conventional geothermobarometry and multi-equilibria geothermobarometry using the THERMOCALC v.3.33 (Supplementary Data, Tables S1 and S2). The garnet-biotite thermometer was used to calculate the temperature condition at a fixed pressure of 8 kbar, and the estimated temperature varies from 747 to 865 °C. The pressure is estimated by the garnet-plagioclase-Al_2SiO_5-quartz geobarometer, which lies at 8.25 kbar. The temperature was determined using a garnet-cordierite geothermometer ranging from 622 to 696 °C, while the pressure was estimated using a garnet-cordierite-sillimanite-quartz geobarometer, which ranges from 5.49 to 6.22 kbar. THERMOCALC software version 3.33 was used to calculate the *P-T* conditions (Powell and Holland, 1988; Holland and Powell, 2011). The P_{av}, T_{av} and PT_{av} were calculated using several metamorphic phases, including independent interactions amongst garnet, cordierite, biotite and plagioclase end-member minerals, and their estimated values

Table 3
Analytical results of zircon geochronology for metapelites using SHRIMP II.

Spot/ YK-4	% $^{206}Pb_c$	Ppm U	ppm Th	Th/U	ppm $^{206}Pb^*$	Age (Ma)#		Discor-dant (%)	Isotope ratio (±%)#				Error correction
						$^{206}Pb/^{238}U$	$^{207}Pb/^{206}Pb$		$^{238}U/^{206}Pb^*$	$^{207}Pb^*/^{206}Pb^*$	$^{207}Pb^*/^{235}U$	$^{206}Pb^*/^{238}U$	
1.1	0.00	201	130	0.65	51.2	1675 ± 11	1696 ± 21	1	3.371 ± 0.73	0.1039 ± 1.2	4.252 ± 1.4	0.2967 ± 0.73	.530
2.1	0.05	237	167	0.71	60.3	1675.1 ± 10	1645 ± 23	−2	3.37 ± 0.68	0.1011 ± 1.2	4.137 ± 1.4	0.2967 ± 0.68	.477
3.1	0.00	282	248	0.88	71.8	1670.4 ± 9.6	1664 ± 21	0	3.381 ± 0.65	0.1022 ± 1.1	4.166 ± 1.3	0.2958 ± 0.65	.503
4.1	0.00	399	277	0.69	97.5	1612.8 ± 9.8	1617 ± 20	0	3.518 ± 0.69	0.0996 ± 1.1	3.905 ± 1.3	0.2843 ± 0.69	.535
5.1	0.00	205	134	0.65	52.3	1678 ± 10	1660 ± 23	−1	3.364 ± 0.71	0.102 ± 1.3	4.179 ± 1.4	0.2973 ± 0.71	.493
6.1	0.00	300	140	0.47	73.7	1622.1 ± 9.4	1613 ± 20	−1	3.495 ± 0.66	0.0994 ± 1.1	3.922 ± 1.3	0.2861 ± 0.66	.523
7.1	0.00	235	183	0.78	59.6	1667 ± 10	1646 ± 22	−1	3.388 ± 0.69	0.1012 ± 1.2	4.119 ± 1.4	0.2952 ± 0.69	.506
8.1	0.12	201	135	0.67	46.1	1521.6 ± 10	1562 ± 27	3	3.756 ± 0.73	0.0967 ± 1.5	3.551 ± 1.6	0.2662 ± 0.73	.449
9.1	0.00	415	263	0.63	99.1	1580.4 ± 9.7	1578 ± 21	0	3.599 ± 0.7	0.0976 ± 1.1	3.737 ± 1.3	0.2778 ± 0.7	.533
10.1	0.04	278	170	0.61	71.1	1676.8 ± 9.7	1670 ± 21	0	3.366 ± 0.66	0.1025 ± 1.1	4.199 ± 1.3	0.2971 ± 0.66	.510
11.1	0.03	338	239	0.71	86.1	1671.6 ± 9.2	1661 ± 19	−1	3.378 ± 0.63	0.102 ± 1	4.165 ± 1.2	0.296 ± 0.63	.530
12.1	0.00	213	150	0.70	54.2	1676 ± 10	1704 ± 23	2	3.369 ± 0.7	0.1044 ± 1.3	4.274 ± 1.4	0.2968 ± 0.7	.484
13.1	0.00	229	144	0.63	58.2	1673 ± 10	1662 ± 22	−1	3.374 ± 0.68	0.102 ± 1.2	4.17 ± 1.4	0.2964 ± 0.68	.498
14.1	0.00	448	335	0.75	114	1673.8 ± 8.8	1659 ± 16	−1	3.373 ± 0.59	0.101 ± 0.85	4.166 ± 1	0.2965 ± 0.59	.573
15.1	0.00	248	180	0.73	62.9	1670 ± 11	1668 ± 21	0	3.381 ± 0.76	0.1024 ± 1.1	4.175 ± 1.4	0.2958 ± 0.76	.551

Errors are 1-sigma; Pb_c and Pb^* indicate the common and radiogenic portions, respectively.
Common Pb corrected using measured ^{204}Pb.

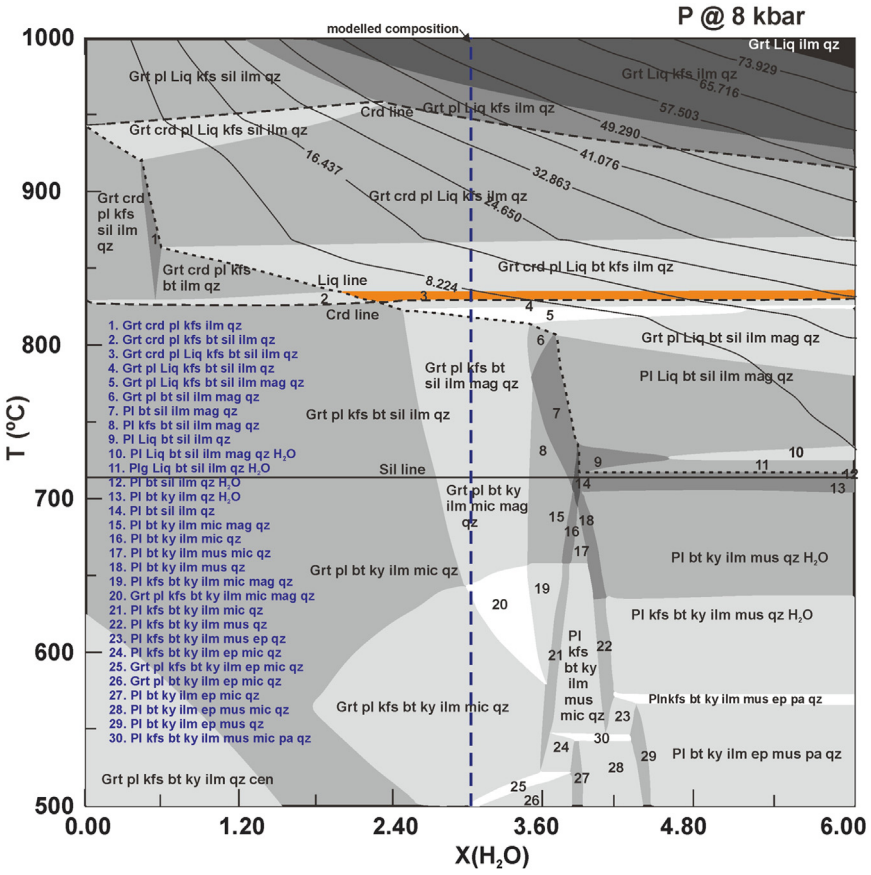

Fig. 10. T–X(H_2O) Pseudosection for metapelite (KT-4) at 8 kbar, showing the effects of varying the molar proportions of bulk-rock H_2O. The white coarse line is solidus, the black dash line represents a field of cordierite bearing phase, and the blue dash line is modelled composition of H_2O (3.01%). Isopleth lines of melt (vol%) are contoured.

were 6.2 ± 2.06 kbar, 682 ± 74 °C and 5.8 ± 1.9 kbar/ 663 ± 87 °C, respectively.

6.2. P-T-X *pseudosection modelling*

The phase equilibria modelling are a very promising tool for constraining the history of metamorphism with various metamorphic stages by bulk rock composition. The metapelites under investigation are made up of layers of leucosomes and melanosomes. The existence of melt is indicated by the presence of a strong leucosome band in these rocks (Fig. 3a). H_2O is found in hydrous mineral phases such as cordierite and biotite, in which cordierite (~1–2 wt% H_2O) and biotite (~5–6 wt% H_2O) constitute about 29% and 9% of the total rock volume, respectively. The T-X(H_2O) pseudosection was calculated at 8.0 kbar pressure (Fig. 10) for metapelite. Based on this observation, the bulk rock composition is estimated to be around ~3.00 mol% H_2O. However, the O_2 was estimated by integrating mineral compositions and the modal abundance of the phases obtained in the rock.

In the NCKFMASHTO phase diagram, the peak metamorphism condition with the mineral assemblage Grt-Bt-Sil-Pl-Kfs-Qz-Liq-Ilm has been estimated at 8.20 kbar and 825 °C (Fig. 11), which is also obtained from conventional geothermobarometry. Biotite combines with Sillimanite + Quartz to generate peritectic garnet during high-grade metamorphism, and biotite is found in the peak assemblage as a result of this dehydration melting process. On the other hand, biotite with high fluorine and TiO_2 content maybe stable in granulite-facies conditions (Bose et al., 2005). Garnet, biotite and sillimanite containing mineral phase are stable at high pressures. In contrast, the low-pressure region in the phase diagram dominates the cordierite bearing assemblage, indicating the decompression reactions (3 & 4). The mineral assemblage of metapelites exhibits the peak metamorphic equilibria at high pressure, followed by isothermal decompression (ITD) path at low pressure. The observed mineral equilibria (Grt-Crd-Bt-Sil-Pl-Kfs-Qz-Ilm-Mag) are considered as a retrograde stage with conventional geothermobarometry estimates of *P-T* condition ranging from 5.49 to 6.22 kbar/ 620–696ºC.

7. Discussions

7.1. Implication of geochemical data and petrogenesis

The geochemical classification schemes of the investigated metapelites and granite gneiss basement rocks show that they are primarily trachy-andesite and andesite in nature. Both rock types have different magmatic ages; metapelites are younger (1672 ± 6 Ma; this study) and granitic gneisses are older (1714 ± 6 Ma; Ghosh et al., 1991, 1994), which were dated from a similar study area around the Sonapahar region of Patharkhang. The distribution of the studied rocks enables to identification of the meta-igneous nature of felsic to intermediate composition; it deduces that all studied samples derived from igneous protoliths (Werner, 1987). Al-rich pellitic with some volcanic intercalations, possibly modified by metamorphic differentiation, were the precursors of cordierite-bearing metapelites. The low P_2O_5, TiO_2, Zr and V contents in metapelites and granitic gneisses, as well as the complex nature of the immobile elements with differentiation, were most likely caused by crystallisation of minor mineral phases from the melt, such as zircon and apatite. The Rb/Sr ratios of metapelites (1.73–2.46) and granite gneisses (1.57–9.53) are both high (Table 2), indicating magmatic evolution. Furthermore, the trace and REEs pat-

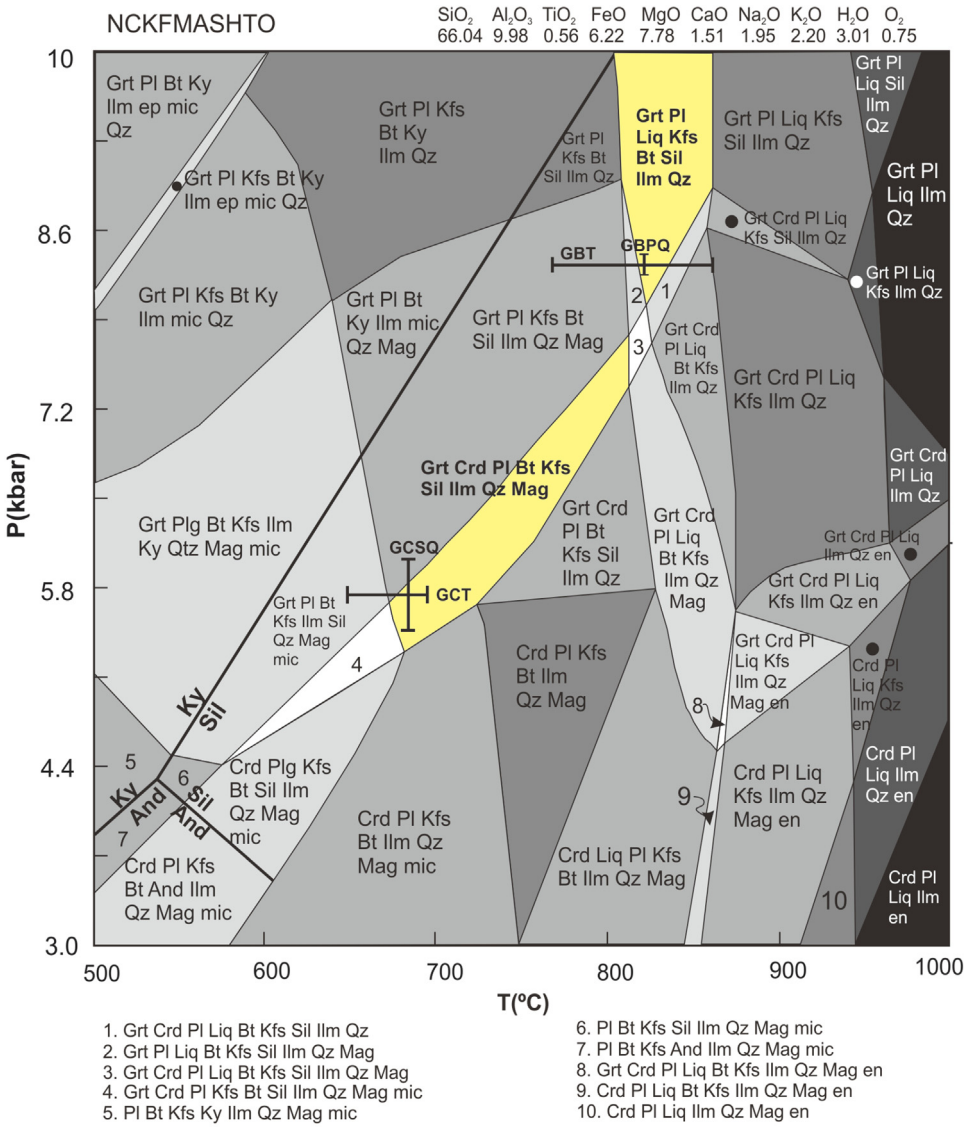

Fig. 11. NCKFMASHTO *P-T* pseudosection for metapelite (KT-4) of Sonapahar showing calculated mineral equilibria for the minerals assemblage grt-crd-pl-sil-kfs-bt-liq-ilm-mag-qz (Mineral abbreviations: Whitney and Evans, 2010). GBT: garnet-biotite thermometry; GBPQ: garnet-biotite-plagioclase-sillimanite-quartz barometer; GCT: garnet-cordierite thermometry; GCSQ: garnet-cordierite-sillimanite-quartz barometer. Source: Supplementary Data, Table S1).

terns of metapelites and granitic gneisses are nearly equal (Fig. 6), the enrichment of Ba, Pb, Rb, Sr, Zn and U in younger metapelites compared to older granite gneisses could be attributed to varying degrees of magmatic evolution. Overall, metapelites and basement rocks show significant enrichment in both LILE and HFSE in the spider diagram. Negative Nb anomalies are common in the continental crust and may indicate crustal participation in magmatic processes (Rollinson, 1993). Both rock types' REE may be revealing of feldspar growth and show a strong fractionation of light REE over heavy REE. The observed negative Eu, Ba and Sr anomalies in both metapelites and granite gneisses suggest that the source was feldspar-depleted or controlled by feldspar fractionations. Due to their migration from the mineral phase to the melt phase during high-grade metamorphism, HFSE and REE are significant elements. Overall geochemical results show enrichment in the LILE and LREE, but relative depletion in Nb and HREE. These characteristics are similar to orogenic belt post-collisional tectonism. It is proposed that the trachy-andesitic magmas were formed by melting sub-continental lithospheric mantle of magmatic origin that had enriched in LILE during previous subduction events. The relationship between HFSE depletion and LILE enrichment suggests that protolith of metapelites and basement granitic gneisses evolved from volcanic arc rocks (Eiler et al., 2000).

7.2. Tectonic settings

According to a combined study of lithological, geochemical, geochronological, and tectono-metamorphic evolution of the SMGC, Sausar, Betul, Chhotanagpur Granite Gneissic Complex (CGGC) and Mahakoshal Belt evolved through the magmatic emplacement that further metamorphosed to the amphibolite to granulite facies condition (Bora and Kumar, 2015; Kumar et al., 2017, 2022a, 2022b; Chatterjee, 2018; Chattopadhyay et al., 2020; Deshmukh and Prabhakar, 2020; Kumar et al., 2022b). Due to the involvement of various geological factors, the condition of magmatism and its metamorphism are important factors in determining tectonic history. A variety of discriminant diagrams have been used to characterise the protolithic character and tectonism of metapelites and basement rocks. The $(Y/Nb)_N$ vs. $(Th/Nb)_N$ discrimination diagram constrained the tectonism associated with

the convergent margins (Fig. 7a). The tectonic discrimination diagrams revealed evidences of magmatism during subduction setting, particularly in the Zr vs. Nb/Zr, Nb vs. Y and Rb vs. (*Y* + Nb). The volcanic arc granite field contains all of the metapelites and granitic gneisses basement rocks. The Bangladesh granitic gneiss and the CGGC's pelitic granulites from the Paleoproterozoic period produce similar results (Hossain et al., 2018; Kumar et al., 2021). The U-Pb SHRIMP dating technique is the most basic tool for determining magmatic emplacement age; in this case, the protolith age is denoted by ca. 1672 Ma, while the M1 stage of metamorphism is denoted by ca. 1571 Ma (Dwivedi et al., 2020). This study obtained ages ranging from ca. 1700 to ca. 1600 Ma, and this period was very prone to magmatic activity, as evidenced by records from the Lesser Himalaya (Kohn et al., 2010), Eastern Ghat Mobile Belt (Bose et al., 2011), Mahakoshal Supracrustal Belt (Yadav et al., 2020), CGGC (Kumar et al., 2021), Yerida Basin (Bagas, 2004), Gascoyne Complex (Sheppard et al., 2005) and Yilgara Craton (Occhipinti et al., 1998).

During the Columbian assembly, numerous metamorphism and deformation were preserved in mafic granulites, pelitic granulites and granitic gneisses in this SMGC (Dwivedi et al., 2020 and references therein). Many continental collision zones have high-grade metamorphic phenomena along a "clockwise" *P-T* path, which may be correlated with supercontinent assembly. The petrography and pseudosection show that the metapelites went through peak metamorphism and then retrograde metamorphism. Garnet crystals coexist with biotite, sillimanite and plagioclase in petrogrpahical domains (Fig. 4a and b). Under high pressure and temperature conditions, the peak metamorphic assemblage (garnet + sillimanite + plagioclase + biotite + quartz + K-feldspar + ilmenite + liquid) was formed (Fig. 11). To achieve peak metamorphism, the reaction Bt + Qz → Grt + Kfs + Melt produces garnet. The presence of garnet, biotite, cordierite, sillimanite, K-feldspar, quartz, plagioclase, ilmenite and magnetite defines the predicted retrograde metamorphism. The matrix cordierite, biotite and plagioclase, which form a late assemblage around the garnet rim, represent this textural evidence (Fig. 4c and e). The Sonapahar region is made up of upper amphibolite to granulite facies regional metamorphic rocks associated with migmatites and other granulitic rocks, with a clockwise *P-T* path trajectory. The NCKFMASHTO system is used to generate a *P-T* phase diagram of metapelites (KT-4). The *P-T* pseudosection with a stable phase, grt-bt-sil-kfs-pl-liq-ilm-qz occurs in a tetravariant field with *P-T* condition 8.25 kbar/ 820 °C. Cordierite-bearing (grt-crd-bt-kfs-pl-sil-qz-ilm-mag) mineral assemblage is stable in the divariant field as pressure decreases, and geothermobarometry predicts *P-T* conditions ranging from 5.49 to 6.22 kbar and 620 to 696 °C (Fig. 11). Cordierite's low-pressure stability is consistent with petrography and mineralogy studies, which show that cordierite forms from the breakdown of garnet and sillimanite. It also supports the texture of decompression seen in petrography, in which garnet breaks down under low pressure to form cordierite. The Paleoproterozoic (ca. 1672 Ma) protolith of metapelites was followed by a Mesoproterozoic (ca. 1571 Ma) peak metamorphic event and Neoproterozoic (ca. 478 Ma) post-peak metamorphism (Dwivedi et al., 2020).

7.3. SMGC position in the columbia assembly

The evolution of the Earth involved multiple cycles of the amalgamation and fragmentation of a supercontinents (Nance et al., 1988). Between ~2000 Ma and ~1800 Ma, the Columbia accreted, and around ca. 1500 Ma, further disintegration processes commenced (Rogers and Santosh, 2002; Zhao et al., 2002, 2004). Tectono-magmatic events have been recorded as Paleoproterozoic geotectonic reconstruction from various regions; CITZ (ca. 1650 Ma: Bhowmik et al., 2014), CGGC (ca. 1700 Ma: Chatterjee and Ghose, 2011), Eastern Ghat Mobile Belt (EGMB) (ca. 1760 Ma: Bose et al., 2011; Dasgupta et al., 2013), SMGC (ca. 1700 Ma: Deshmukh et al., 2017: Kumar et al., 2017) and Aravalli-Delhi Mobile Belt (ca. 1700 Ma: Bhowmik et al., 2010). The CITZ preserves Paleoproterozoic (Sausar, 1800–1600 Ma; Betul, ~1550 Ma; CGGC, ~1650 Ma; Mahakoshal, ~1700 Ma) orogenic events. Finally, a last collision events was occurred in the Neoproterozoic (ca. 1040–930 Ma), resulting in the stitching of the Northern and Southern Indian blocks (Deshmukh et al., 2017; Chattopadhyay et al., 2019; Dey et al., 2019). Santosh et al. (2004) dated EGMB granulites at ca. 1700–1600 Ma, implying that the Paleoproterozoic rift basin was expanding during this period. This rift basin has the same signature as the rift in the Columbia region of Western Australia. The CITZ is a collision boundary in the Indian shield where the Northern and Southern Indian Blocks collided and merged in Paleoproterozoic time, forming the Columbia supercontinent configuration. The basement rock on the Meghalaya Plateau is granitic-gneiss, with an age of ca. 1700 Ma (Ghosh et al., 1991) and magmatic activities occurred in the same rock type between 1600 and 1100 Ma (Yin et al., 2010). The metapelites in this study have a Paleoproterozoic age (1672 ± 6 Ma), which clearly shows that the CITZ and EGMB were extended in the SMGC during the Columbian assembly. The Columbia supercontinent is constituted of Eastern India (SMGC and EGMB), East Antarctica and Western Australia (Rogers and Santosh, 2002). Because of the heavier ice cap cover, the geology of East Antarctica is less well studied. However, recent research has revealed that the Trans-antarctic Mountain, Wilkes Land's basement and their marginal portion are linked to the Paleoproterozoic granitoid and Mesoproterozoic mafic igneous rocks of Australian cratons, namely Gawler and Curnamona (Goodge et al., 2001; Peucat et al., 1999, 2002). The Capricorn

Fig. 12. The schematic map shows the Columbia supercontinent with the SMGC as a continuation of the CITZ (modified after Rogers and Santosh, 2002). Abbreviations of orogens: Ad, Aravalli-Delhi; Af, Albany-Fraser; Ca, Capricorn; CITZ, Central Indian Tectonic Zone; Eg, Eastern Ghat Belt; Ra, Rayner; SMGC, Shillong-Meghalaya Gneissic Complex; Wb, Windmill Islands–Bunger Hills.

orogeny defines a collisional frontier between the Pilbara and the Yilgarn cratons in Western Australia. The Yerrida, Bryah and Padbury basins have metamorphosed basements as well as volcano-sedimentary basins (Cawood and Tyler, 2004). The Padbury Basin was produced as a foreland setting over the Bryah Basin, whilst the rest of the basins were developed in a back-arc setting between ~2100 and ~2000 Ma (Woodhead and Hergt, 1997; Pirajno and Occhipinti, 1998; Martin and Thorne, 2004). The closing of the basin was observed between the Pilbara and Yilgram cratons during the Capricorn orogeny (ca. 2000–1800 Ma; Occhipinti et al., 1998; Bagas, 2004). During the Yapungku orogeny (ca. 1660–1790 Ma), the Yerrida Basin was deformed and metamorphosed (Bagas, 2004; Pirajno et al., 2004). These findings suggest that the Capricorn orogeny's tectonic episodes at ca. 1800–1600 Ma are similar to those found in the CITZ (Mohanty, 2010, 2012). Granulites from southern EGMB rift basins (Santosh et al., 2004) are Paleoproterozoic in age and have a similar configuration to the Columbia region of western North America (Rogers and Santosh, 2002; Fig. 12).

8. Conclusions

This investigation contributes to the petrochronological and geochemical evolution of metapelites and granitic gneiss basement rocks from the SMGC's Sonapahar region. According to SHRIMP U-Pb zircon dating, the protolith age of the Sonapahar metapelites is ca. 1672 Ma, while the first stage of metamorphism was reported to be ca. 1571 Ma. Peak metamorphic conditions of metapelites were recorded using the NCKFMASHTO system at 8.25 kbar/ 820 °C. The results define an isothermal decompression retrogressive *P-T* path, where the peak condition is grt + sil + bt + pl + qz, and then it follows the isothermal decompression (ITD) path to achieve grt + bt + crd + sil + pl + kfs + qz assemblages at 5.8 kbar/ 680 °C *P-T* condition. The Y vs. Nb and (*Y* + Nb) vs. Rb diagram indicates that the metapelites and granitic gneiss basement rocks have an affinity towards the volcanic arc granite and developed as convergent margin rocks during subduction setting. The magma is produced by the melting of the subducted oceanic crust during syn-collisional activity in a volcanic arc context.

Declaration of Competing Interest

The authors declare no conflicts of interest.

CRediT authorship contribution statement

Shyam Bihari Dwivedi: Conceptualization, Supervision, Writing – review & editing. **Pratigya Pathak:** Conceptualization, Writing – original draft, Writing – review & editing. **Kevilhoutuo Theunuo:** Investigation. **Ravi Ranjan Kumar:** Conceptualization, Writing – original draft, Writing – review & editing.

Acknowledgements

S.B. Dwivedi thanks the DST (India) for sponsoring project ESS/16/304/2005 for financial support. We're also obliged to the Director of the IIT (BHU), Varanasi (India) for providing infrastructure. We would like to thank Vinod Samuel (Associate Editor) and the reviewers for their constructive comments, which helped to improve the manuscript's quality.

Supplementary materials

Supplementary material associated with this article can be found, in the online version, at doi:10.1016/j.geogeo.2022.100161.

References

Acharyya, S.K., Mitra, N.D., Nandy, D.R., 1986. Regional geology and tectonic setting of North-East India and adjoining region. Geology of Nagaland Ophiolite. G.B. Ghose Commemorative Volume. (A Compilation of Research Papers on Nagaland Ophiolites). Mem. Geol. Sur. India 119, 6–12.

Acharyya, S.K., 2003. The nature of Mesoproterozoic Central India Tectonic Zone with exhumed and reworked older granulites. Gondawana Res 6 (2), 197–214. doi:10.1016/S1342-937X(05)70970-9.

Ameen, S.M.M., Wilde, S.A., Kabir, M.Z., Akon, E., Chowdhury, K.R., Khan, M.S.H., 2007. Paleoproterozoic granitoids in the basement of Bangladesh: a piece of the Indian shield or an exotic fragment of the Gondwana jigsaw? Gondawana Res 12 (4), 280–387. doi:10.1016/j.gr.2007.02.001.

Bagas, L., 2004. Proterozoic evolution and tectonic setting of the northwest Paterson Orogen. Western Australia. Precambr. Res. 128, 475–496. doi:10.1016/j.precamres.2003.09.011.

Bhowmik, S.K., Sarbadhikari, A.B., Spiering, B., Raith, M., 2005. Mesoproterozoic reworking of Paleoproterozoic ultrahigh-temperature granulites in the Central Indian Tectonic Zone and its implications. J. Petrol. 46 (6), 1085–1119. doi:10.1093/petrology/egi011.

Bhowmik, S.K., Bernhardt, H.J., Dasgupta, S., 2010. Grenvillian age high-pressure upper amphibolite-granulite metamorphism in the Aravalli-Delhi Mobile Belt, Northwestern India: new evidence from monazite chemical age and its implication. Precambr. Res. 178 (1–4), 168–184. doi:10.1016/j.precamres.2010.02.015.

Bhowmik, S.K., Wilde, S.A., Bhandari, A., Pal, T., Pant, N.C., 2012. Growth of the Greater Indian landmass and its assembly in Rodinia: geochronological evidence from the Central Indian Tectonic Zone. Gondawana Res 22 (1), 54–72. doi:10.1016/j.gr.2011.09.008.

Bhowmik, S.K., Wilde, S.A., Bhandari, A., Sarbadhikari, A.B., 2014. Zoned Monazite and Zircon as Monitors for the thermal history of granulite Terraines: an example from the central Indian Tectonic Zone. J. Petrol. 55 (3), 585–621. doi:10.1093/petrology/egt078.

Bidyananda, M., Deomurari, M.P., 2007. Geochronological constraints on the evolution of Meghalaya massif, northeastern India: an ion microprobe study. Curr. Sci. 93 (11), 1620–1623.

Bora, S., Kumar, S., 2015. Geochemistry of biotites and host granitoid plutons from the Proterozoic Mahakoshal Belt, central India tectonic zone: implication for nature and tectonic setting of magmatism. Int. Geol. Rev. 57 (11–12), 1686–1706. doi:10.1080/00206814.2015.1032372.

Bose, S., Das, K., Fukuoka, M., 2005. Fluorine content of biotite in granulite-grade metapelitic assemblages and its implications for the Eastern Ghats granulites. European J. Mineral. 17, 665–674. doi:10.1127/0935-1221/2005/0017-0665.

Bose, S., Dunkley, D.J., Dasgupta, S., Das, K., Arima, M., 2011. India–Antarctica–Australia–Laurentia connection in the Paleoproterozoic–Mesoproterozoic revisited: evidence from new zircon U–Pb and monazite chemical age data from the Eastern Ghats Belt. India. Bull. Geol. Soc. America. 123 (9–10), 2031–2049. doi:10.1130/B30336.1.

Cawood, P.A., Tyler, I.M., 2004. Assembling and reactivating the Proterozoic Capricorn Orogen: lithotectonic elements, orogenies, and significance. Precambr. Res. 128, 201–218. doi:10.1016/j.precamres.2003.09.001.

Chatterjee, N., 2018. An assembly of the Indian Shield at c. 1.0 Ga and shearing at c. 876–784 Ma in Eastern India: insights from contrasting *P-T* paths, and burial and exhumation rates of metapelitic granulites. Precambr. Res. 317, 117–136. doi:10.1016/j.precamres.2018.08.024.

Chatterjee, N., Ghose, N.C., 2011. Extensive early Neoproterozoic high-grade metamorphism in North Chhotanagpur gneissic complex of the Central Indian Tectonic Zone. Gondawana Res 20 (2–3), 362–379. doi:10.1016/j.gr.2010.12.003.

Chatterjee, N., Mazumder, A.C., Bhattacharya, A., Saikia, R.R., 2007. Mesoproterozoic granulites of the Shillong-Meghalaya Plateau: evidence of westward continuation of the Prydz Bay Pan-African suture into Northeastern India. Precambr. Res. 152 (1–2), 1–26. doi:10.1016/j.precamres.2006.08.011.

Chatterjee, N., Bhattacharya, A., Duarah, B.P., Mazumdar, A.C., 2011. Late Cambrian reworking of Paleo-Mesoproterozoic granulites in Shillong–Meghalaya Gneissic complex (Northeast India): evidence from PT pseudosection analysis and monazite chronology and implications for East Gondwana assembly. J. Geol. 119, 311–330. doi:10.1086/659259.

Chattopadhyay, A., Bhowmik, S.K., Roy, A., 2019. Tectonothermal evolution of the Central Indian Tectonic Zone and its implications for Proterozoic supercontinent assembly: the current status. Episodes J. Int. Geosci. 43 (1), 132–144. doi:10.18814/epiiugs/2020/020008.

Chattopadhyay, A., Bhowmik, S., Roy, A., 2020. Tectonothermal evolution of the Central Indian Tectonic Zone and its implications for Proterozoic supercontinent assembly: the current status. Episodes 43, 132–144. doi:10.18814/epiiugs/2020/020008.

Condie, K.C., 2004. Supercontinents and superplume events: distinguishing signals in the geologic record. Phy. Earth Planet Int. 146 (1–2), 319–332. doi:10.1016/j.pepi.2003.04.002.

Connolly, J.A.D., 2005. Computation of phase equilibria by linear programming: a tool for geodynamic modeling and its application to subduction zone decarbonation. Earth Planet Sci. Lett. 236 (1–2), 524–541. doi:10.1016/j.epsl.2005.04.033.

Connolly, J.A.D., 2009. The geodynamic equation of state: what and how. Geochem. Geophy. Geosys. 10 (10), 1–19. doi:10.1029/2009GC002540.

Dasgupta, S., Bose, S., Das, K., 2013. Tectonic evolution of the Eastern Ghats Belt. India. Precambr. Res. 227, 247–258. doi:10.1016/j.precamres.2012.04.005.

Desikachar, S.V., 1974. A review of the tectonic and geological history of Eastern India in terms of 'plate tectonic' theory. J. Geol. Soc. India. 15 (2), 137–149.

Deshmukh, T., Prabhakar, N., 2020. Linking collision, slab break-off and subduction polarity reversal in the evolution of the Central Indian Tectonic Zone. Geol. Mag. 157 (2), 340–350. doi:10.1017/S0016756819001419.
Deshmukh, T., Prabhakar, N., Bhattacharya, A., Madhavan, K., 2017. Late Paleoproterozoic clockwise *P–T* history in the Mahakoshal Belt, Central Indian Tectonic Zone: implications for Columbia supercontinent assembly. Precambr. Res. 298, 56–78. doi:10.1016/j.precamres.2017.05.020.
Dey, A., Karmakar, S., Mukherjee, S., Sanyal, S., Dutta, U., Sengupta, P., 2019. High Pressure metamorphism of mafic granulites from the Chotanagpur Granite Gneiss Complex, India: evidence for collisional tectonics during assembly of Rodinia. J. Geodyn. 129, 24–43. doi:10.1016/j.jog.2019.03.005.
Dunn, J.A., 1929. The aluminous refractory minerals: kyanite, sillimanite, and corundum in Northern India. Mem. Geol. Sur. India. 52, 1–165.
Dwivedi, S.B., Theunuo, K., 2011. Two-pyroxene bearing Granulites from Patharkhang, Shillong-Meghalaya Gneissic Complex (SMGC). Curr. Sci. 100, 100–105.
Dwivedi, S.B., Theunuo, K., 2013. Petrology and geochemistry of Metapelites and Basic granulite from the Sonapahar region of Shillong Meghalaya Gneissic Complex, North East India. J. Geol. Soc. India. 81 (6), 755–766.
Dwivedi, S.B., Theunuo, K., 2017. Occurrence of Wagnerite in Mg-Al granulites of Sonapahar Meghalaya. J. Earth Sys. Sci. 126 (4), 52. doi:10.1007/s12040-017-0829-8.
Dwivedi, S.B., Theunuo, K., Kumar, R.R., 2020. Characterization and metamorphic evolution of Mesoproterozoic granulites from Sonapahar (Meghalaya), NE-India, using EPMA monazite dating. Geol. Mag. 1, 1–19. doi:10.1017/S0016756819001389.
Eiler, J., Crawford, A., Elliott, T., Farley, K.A., Valley, J.W., Stolper, E.M., 2000. Oxygen isotope geochemistry of oceanic arc lavas. J. Petrol. 41 (2), 229–256. doi:10.1093/petrology/41.2.229.
Evans, P., 1964. The tectonic framework of Assam. J. Geol. Soc. India. 5, 80–96.
Ghosh, S., Bhalla, J.K., Paul, D.K., Sarkar, A., Bishui, P.K., Gupta, S.N., 1991. Geochronology and geochemistry of granite plutons from East Khasi Hills. Meghalaya. J. Geol. Soc. India. 37, 331–342.
Ghosh, S., Chakraborthy, S., Paul, D.K., Bhalla, J.K., Bishui, P.K., Gupta, S.N., 1994. New Rb-Sr ages and geochemistry of granitoids from Meghalaya and their significance in middle-late Proterozoic crustal evolution. In: Indian Miner., 48, pp. 33–44.
Ghosh, S., Fallick, A.E., Paul, D.K., Potts, P.J., 2005. Geochemistry and origin of Neoproterozoic granitoids of Meghalaya, northeast India: implications for linkage with amalgamation of Gondwana supercontinent:. gondwana Res 8, 421–432. doi:10.1016/S1342-937X(05)71144-8.
Goodge, J.W., Fanning, C.M., Bennett, V.C., 2001. U-Pb evidence of ~1.7 Ga crustal tectonism during the Nimrod Orogeny in the Transantarctic Mountains, Antarctica; implications for Proterozoic plate reconstructions. Precambr. Res. 112 (3–4), 261–288. doi:10.1016/S0301-9268(01)00193-0.
Harley, S.L., 1989. The origins of granulites: a metamorphic perspective. Geol. Mag. 126, 215. doi:10.1017/S0016756800022330.
Harris, L.B., 1995. Correlation between the Albany, Fraser, and darling mobile belts of Western Australia and Mirnyy to Windmill Islands in the east antarctic shield: implications for proterozoic gondwanaland reconstructions. In: Yoshida, Y., Santosh, M., (eds) India and Antarctica during the Precambrian. Mem. Geol. Soc. India 34, 73–100.
Holland, T., Powell, R., 2003. Activity–composition relations for phases in petrological calculations: an asymmetric multi-component formulation. Contrib. Mineral Petrol. 145 (4), 492–501. doi:10.1007/s00410-003-0464-z.
Holland, T.J.B., Powell, R., 2011. An improved and extended internally consistent thermodynamic dataset for phases of petrological interest, involving a new equation of state for solids. J. Metamorph. Geol. 29, 333–383. doi:10.1111/j.1525-1314.2010.00923.x.
Hossain, I., Tsunogae, T., Rajesh, H.M., Chen, B., Arakawa, Y., 2007. Paleoproterozoic U-Pb SHRIMP zircon age from basement rocks in Bangladesh: a possible remnant of the Columbia supercontinent. Com. Rend. Geosci. 339 (16), 979–986. doi:10.1016/j.crte.2007.09.014.
Hossain, I., Tsunogae, T., Tsutsumi, Y., Takahashi, K., 2018. Petrology, geochemistry and LA-ICP-MS U-Pb geochronology of Paleoproterozoic basement rocks in Bangladesh: an evaluation of calc-alkaline magmatism and implication for Columbia supercontinent amalgamation. J. Asian Earth Sci. 157, 22–39. doi:10.1016/j.jseaes.2017.09.016.
Khanna, P.P., Saini, N.K., Mukherjee, P.K., Purohit, K.K., 2009. An appraisal of ICP-MS technique for determination of REEs: long term QC assessment of Silicate Rock Analysis. J. Himalayan Geol. 30 (1), 95–99.
Kohn, M., Paul, S.K., Corrie, S.L., 2010. The lower Lesser Himalayan sequence: a Paleoproterozoic arc on the northern margin of the Indian plate. Bull. Geol. Soc. America. 122, 323–335. doi:10.1130/B26587.1.
Kumar, R., Kawaguchi, K., Dwivedi, S.B., Das, K., 2021. Metamorphic evolution of the pelitic and mafic granulites from Daltonganj, Chhotanagpur Granite Gneiss Complex, India: constraints from zircon U–Pb age and phase equilibria modelling. Geol. J. 57 (3), 1284–1310. doi:10.1002/gj.4340.
Kumar, R., Dwivedi, S.B., Pathak, P., 2022a. Phase equilibria modelling and geochemistry of high-grade gneiss from the Chhotanagpur Granite Gneiss Complex, eastern India: implications for tectono-metamorphic evolution. Geosys. Geoenv. 1 (4), 100082. doi:10.1016/j.geogeo.2022.100082.
Kumar, S., Pundir, S., Rino, V., Bora, S., Pathak, M., Anettsungla, Joshi, H., Rawat, M.S., Pieru, T., Singh, K.M., 2022b. Geochemistry of Proterozoic and Cambrian granites from Meghalaya Plateau, north-east India: implication on petrogenesis of post-collisional, transitional from I-type to A-type felsic magmatism. Geol. J. 57 (4), 1476–1510. doi:10.1002/gj.4351.
Kumar, S., Rino, V., Hayasaka, Y., Kimura, K., Raju, S., Terada, K., Pathak, M., 2017. Contribution of Columbia and Gondwana supercontinent assembly and growth-related magmatism in the evolution of the Meghalaya Plateau and the Mikir Hills, Northeast India: constraints from U–Pb SHRIMP zircon geochronology and geochemistry. Lithos 277, 356–377. doi:10.1016/j.lithos.2016.10.020.
Lal, R.K., Ackermand, D., Seifert, F., Haldar, S.K., 1978. Chemographic relationships in sapphirine-bearing rocks from Sonapahar, Assam, India. Contrib. Mineral Petrol. 67, 169–187. doi:10.1007/BF01046574.
Ludwig, K.R., 2011. Isoplot 3.70 (version-4): a Geochronological Toolkit for Microsoft Excel. Berkeley Chronology Center, Berkeley, California, Spec. Publ. 4.
Martin, D.Mc.B., Thorne, A.M., 2004. Tectonic setting and basin evolution of the Bangemall Supergroup in the northwestern Capricorn Orogen. Precambr. Res. 128, 385–409. doi:10.1016/j.precamres.2003.09.009.
Mazumdar, S.K., 1976. A summary of the precambrian geology of the Khasi Hills, Meghalaya. Geol. Sur. India. Miscell. Publ. 23, 311–334.
Mazumder, S.K., 1986. The Precambrian framework of part of the Khasi Hills, Meghalaya. Geol. Sur. India. Rec. 117, 1–59.
McLennan, S.M., Taylor, S.R., 1980. Th and U in sedimentary rocks: crustal evolution and sedimentary recycling. Nature 285, 621–624. doi:10.1038/285621a0.
Mishra, D.C., Singh, B., Tiwari, V.M., Gupta, S.B., Rao, M.V.S.V., 2000. Two cases of continental collision and related tectonics during the Proterozoic period in Indian sights from gravity modeling constrained by seismic and magnetotelluric studies. Precambr. Res. 99, 149–169. doi:10.1016/S0301-9268(99)00037-6.
Mitra, S.K., 1998. Structure, sulphide mineralization and age of the Shillong group of rocks, Meghalaya. In M.S. Krishnan Commemorative National Seminar. Kolkata, pp. 118–119.
Mohanty, S., 2010. Tectonic evolution of the Satpura mountain belt: a critical evaluation and implication on supercontinent assembly. J Asian Earth Sci 39. doi:10.1016/j.jseaes.2010.04.025, 516-428.
Mohanty, S., 2012. Spatio-temporal evolution of the Satpura Mountain Belt of India: a comparison with the Capricorn Orogen of Western Australia and implication for the evolution of the supercontinent Columbia. Geosci. Front. 3 (3), 241–267. doi:10.1016/j.gsf.2011.10.005.
Moreno, J.A., Molina, J.F., Montero, P., Abu Anbar, M., Scarrow, J.H., Cambeses, A., Bea, F., 2014. Unraveling sources of A-type magmas in juvenile continental crust: constraints from compositionally diverse Ediacaran post-collisional granitoids in the Katerina Ring Complex, southern Sinai, Egypt. Lithos 192-195, 56–85. doi:10.1016/j.lithos.2014.01.010.
Naganjaneyulu, K., Santosh, M., 2010. The Central India Tectonic Zone: a geophysical perspective on continental amalgamation along a Mesoproterozoic suture. Gondawana Res 18 (4), 547–564. doi:10.1016/j.gr.2010.02.017.
Nandy, D.R., 2001. Geodynamics of the Northeastern India and the Adjoining Region. ABC. Publications, Kolkata, p. 209p.
Nance, R.D., Worsley, T.R., Moody, J.B., 1988. The supercontinent cycle. Sci. American. 256, 72–79. doi:10.1038/scientificamerican0788-72.
Occhipinti, S.A., Sheppard, S., Nelson, D.R., Myers, J.S., Tyler, I.M., 1998. Syntectonic granite in the southern margin of the Palaeoproterozoic Capricorn Orogen, Western Australia. Australian J. Earth Sci. 45, 509–512. doi:10.1080/08120099808728408.
Ozha, M.K., Mishra, B., Hazarika, P., Jeyagopal, A.V., Yadav, G.S., 2016. EPMA monazite geochronology of the basement and supracrustal rocks within the Pur-Banera basin, Rajasthan: evidence of Columbia breakup in Northwestern India. J. Asian Earth Sci. 117, 284–303. doi:10.1016/j.jseaes.2015.12.016.
Pearce, J.A., Harris, N.B.W., Tindle, A.G., 1984. Trace element discrimination diagrams for the Tectonic Interpretation of Granitic Rocks. J. Petrol. 25, 956–983. doi:10.1093/petrology/25.4.956.
Peucat, J.J., Meno, R.P., Monnier, O., Fanning, C.M., 1999. The Terre Adélie basement in the East-Antarctica shield: geological and isotopic evidence for a major 1.7 Ga thermal event; comparison with the Gawler craton in South Australia. Precambr. Res. 94, 205–224. doi:10.1016/S0301-9268(98)00119-3.
Peucat, J.J., Capdevila, R., Fanning, C.M., Menot, R.P., Pecora, L., Testut, L., 2002. 1.60 Ga felsic volcanic blocks in the moraines of the Terre Adélie craton, Antarctica: comparisons with the Gawler Ranges Volcanics, South Australia. Australian J. Earth Sci. 49, 831–845. doi:10.1046/j.1440-0952.2002.00956.x.
Pidgeon, R.T., Aftalion, M., 1978. Cogenetic and inherited zircon U-Pb systems in Paleozoic granites of Scotland and England. In: D.R. Bowes, and B.E. Leake, eds. Crustal evolution in northwest Britain and adjacent regions. Geol. J. Spec. Issue. 10, 183–220.
Pirajno, F., Jones, J.A., Hocking, R.M., Halilovic, J., 2004. Geology and tectonic evolution of Palaeoproterozoic basins of the eastern Capricorn Orogen, Western Australia:. precambr. Res. 128 (3–4), 315–342. doi:10.1016/j.precamres.2003.09.006.
Pirajno, F., Occhipinti, S.A., 1998. Geology of the Bryah 1:100 000 sheet: geological survey of Western Australia, 1:100 000 Geological Series Explanatory Notes, 41p.
Powell, R., Holland, T.J.B., 1988. An internally consistent dataset with uncertainties and correlations; 3, Applications to geobarometry, worked examples and a computer program. J. Metamorph. Geol. 6, 173–204. doi:10.1111/j.1525-1314.1988.tb00415.x.
Powell, R., Holland, T.J.B., 1999. Relating formulations of the thermodynamics of mineral solid solutions: activity modelling of pyroxenes, amphiboles, and micas. Am. Mineral. 84, 1–14.
Ray Barman, T., Bishui, P.K., Mukhopadhyay, Ray, J.N., 1990. Rb–Sr geochronology of the high-grade rocks from Purulia, West Bengal and Jamua–Dumka sector, Bihar.

Indian Mineral. 48, 45–60.
Rogers, J.J.W., Santosh, M., 2002. Configuration of Columbia, a Mesoproterozoic supercontinent. Gondawana Res 5, 5–22. doi:10.1016/S1342-937X(05)70883-2.
Rollinson, H.R., 1993. Using Geochemical Data: Evaluation, Presentation, Interpretation. Addison Wesley Longman, Harlow.
Saini, N.K., Mukherjee, P.K., Rathi, M.S., Khanna, P.P., Purohit, K.K., 1998. A new geochemical reference sample of granite (DH-G) from Dalhousie, Himachal Himalaya. J. Geol. Soc. India. 52, 603–606.
Santosh, M., Yokoyama, K., Acharyya, S.K., 2004. Geochronology and tectonic evolution of karimnagar and Bhopalpatnam granulite belts, Central India. Gondawana Res. 7 (2), 501–518. doi:10.1016/S1342-937X(05)70801-7.
Sheppard, S., Occhipinti, S.A., Nelson, D.R., 2005. Intracontinental reworking in the Capricorn Orogen, Western Australia: the 1680–1620 Ma Mangaroon Orogeny. Australian J. Earth Sci. 52 (3), 443–460. doi:10.1080/08120090500134589.
Srivastava, R.K., Guarino, V., Wu, F.Y., Melluso, L., Sinha, A.K., 2019. Evidence of subcontinental lithospheric mantle sources and open-system crystallization processes from in-situ U–Pb ages and Nd–Sr–Hf isotope geochemistry of the Cretaceous ultramafic-alkaline-(carbonatite) intrusions from the Shillong Plateau, north-eastern India. Lithos 330, 108–119. doi:10.1016/j.lithos.2019.02.009.
Sun, S.S., McDonough, W.F., 1989. Chemical and isotopic systematics of oceanic basalts: implications for mantle composition and processes. In: Saunders, A.D., Norry, M.J. (Eds.), Magmatism in the Ocean Basins. Geol. Soc. London. Spec. Publ. 42, 313–345. doi:10.1144/GSL.SP.1989.042.01.19.
Tang, L., Santosh, M., Tsunogae, T., 2019. Petrology, phase equilibria modelling and zircon U-Pb geochronology of garnet-bearing charnockites from the Miyun area: implications for microblock amalgamation of the North China Craton. Lithos. 324-325, 234–245. doi:10.1016/j.lithos.2018.11.012.
Thieblemont, D., Tegyey, M., 1994. Geochemical discrimination of differentiated magmatic rocks attesting for the variable origin and tectonic setting of calc-alkaline magmas. CompteRend De Acad. Des. Sci. Ser. II. 319, 87–94.
Werner, C.D., 1987. Saxonian granulites-igneous or lithoigneous: a contribution to the geochemical diagnosis of the original rock in high metamorphic complexes. ZfS-Mitteilungen 133, 221–250.
White, R.W., Powell, R., Holland, T.J.B., Worley, B., 2000. The effect of TiO_2 and Fe_2O_3 on metapelitic assemblages at greenschist and amphibolite facies conditions: mineral equilibria calculations in the system K_2O-FeO-MgO-Al_2O_3-SiO_2-H_2O-TiO_2-Fe_2O_3. J. Metamorph. Geol. 18 (5), 497–511. doi:10.1046/j.1525-1314.2000.00269.x.
White, R.W., Powell, R., Holland, T.J.B., 2007. Progress relating to the calculation of partial melting equilibria for metapelites. J. Metamorph. Geol. 25 (5), 511–527. doi:10.1111/j.1525-1314.2007.00711.x.
Whitney, D.L., Evans, B.W., 2010. Abbreviations for names of rock-forming minerals. Am. Mineral. 95 (1), 185–187. doi:10.2138/am.2010.3371.
Wiedenbeck, M., Allé, P., Corfu, F., Griffin, W.L., Meier, M., Oberli, F., von Quadt, A., Roddick, J.C., Spiegel, W., 1995. Three natural zircon standards for U-Th-Pb, Lu-Hf, trace element, and REE analyses. Geostand. Newslet. 19 (1), 1–23. doi:10.1111/j.1751-908X.1995.tb00147.x.
Winchester, J.A., Floyd, P.A., 1977. Geochemical discrimination of different magma series and their differentiation products using immobile elements. Chem. Geol. 20, 325–343. doi:10.1016/0009-2541(77)90057-2.
Woodhead, J.D., Hergt, J.M., 1997. Application of the 'double spike' technique to Pb-isotope geochronology. Chem. Geol. 138, 311–321. doi:10.1016/S0009-2541(97)00013-2.
Yadav, B.S., Ahmad, T., Kaulina, T., Bayanova, T., Bhutani, R., 2020. Origin of post-collisional A-type granites in the Mahakoshal Supracrustal Belt, Central Indian Tectonic Zone, India: zircon U-Pb ages and geochemical evidences. J Asian Earth Sci 191, 104247. doi:10.1016/j.jseaes.2020.104247.
Yedekar, D.B., Jain, S.C., Nair, K.K.K., Dutta, K.K., 1990. The Central Indian collision suture. Precambrian of Central Indian. Geol. Sur. India. Spec. Publ. 28, 1–37.
Yin, A., Dubey, C.S., Webb, A.A.G., Kelty, T.K., Grove, M., Gehrels, G.E., Burgess, W.P., 2010. Geologic correlation of the Himalayan orogen and Indian craton: part 1. Structural Geology, U-Pb Zircon geochronology and tectonic evolution of the Shillong plateau and its neighboring regions in NE India. Bull. Geol. Soc. America. 122 (3–4), 336–359. doi:10.1130/B26460.1.
Zhao, G., Cawood, P.A., Wilde, S.A., Sun, M., 2002. Review of global 2.1–1.8 Gaorogens: implications for a pre-Rodinia supercontinent. Earth Sci. Rev. 59, 125–162. doi:10.1016/S0012-8252(02)00073-9.
Zhao, G., Sun, M., Wilde, S.A., Li, S.Z., 2004. A Paleo-Mesoproterozoic supercontinent: assembly, growth, and breakup. Earth Sci. Rev. 67 (1–2), 91–123. doi:10.1016/j.earscirev.2004.02.003.